

DPIImageBench: A Unified Benchmark for Differentially Private Image Synthesis

Chen Gong[†], Kecen Li[†], Zinan Lin[§], Tianhao Wang
University of Virginia, [§]Microsoft Research

Abstract—Differentially private (DP) image synthesis aims to generate artificial images that retain the properties of a sensitive image dataset while protecting the privacy of individual images within the dataset. Despite recent advancements, we find that inconsistent—and sometimes flawed—evaluation protocols have been applied across studies. This not only impedes the understanding of current methods but also hinders future advancements in the field.

To address the issue, this paper introduces **DPIImageBench** for DP image synthesis, with thoughtful design across several dimensions: (1) *Methods*. We study twelve prominent methods and systematically characterize each based on model architecture, pretraining strategy, and privacy mechanism. (2) *Evaluation*. We include nine datasets and seven fidelity and utility metrics to thoroughly assess these methods. Notably, we find that the common practice of selecting downstream classifiers based on the highest accuracy on the sensitive test set not only violates DP but also overestimates the utility scores. **DPIImageBench** corrects for these mistakes. (3) *Platform*. Despite the wide variety of methods and evaluation protocols, **DPIImageBench** provides a standardized interface that accommodates current and future implementations within a unified framework. With **DPIImageBench**, we have several noteworthy findings. For example, contrary to the common wisdom that pretraining on public image datasets is usually beneficial, we find that the distributional similarity between pretraining and sensitive images significantly impacts the performance of the synthetic images and does not always yield improvements. In addition, adding noise to low-dimensional features, such as the high-level characteristics of sensitive images, is less affected by the privacy budget compared to adding noise to high-dimensional features, like weight gradients. The former methods perform better than the latter under a low privacy budget, like 0.2. The source code is available.¹

1. Introduction

Privacy-preserving synthetic data aims to generate artificial data that maintains the properties of real data, enabling data sharing within and across organizations while minimizing privacy risks [1], [2]. Differentially private (DP) dataset synthesis [1], [3] provides a theoretical guarantee to quantify privacy leakage of real data using the synthetic dataset. In recent years, there has been significant development of DP

dataset synthesis methods across various domains, including images [4], [5], [6], tabular data [7], [8], text [9], [10], [11], networking data [12], [13], [14] and more.

Among them, DP image synthesis has witnessed impressive progress [4], [5], [6], [15], [16], [17], [18], [19] but lacks a comprehensive understanding of the strengths and weaknesses of existing synthesizers. While there are several studies summarizing advances in this field, they either focus on discussions [1], [20] and do not perform much evaluation, or only cover subfields [21], [22]. This paper focuses on benchmarking DP image dataset synthesis, addressing several challenges:

- *Platform*: The complex codebases from different methods make it challenging to evaluate different methods easily. For example, failing to standardize the pretraining dataset and model architectures may lead to unfair comparisons.
- *Evaluation*: The lack of unified metrics makes it difficult to evaluate the quality of synthetic images. Existing methods such as PE [5] and PrivImage [4] both utilize FID [23] for fidelity evaluation. However, FID does not assess whether the generated images align with human perception, as described in Section 5.3.2. Even worse, the standard practice that evaluates synthetic image quality by tuning classifiers on the *sensitive test set* to select optimal parameters (used in several methods [15], [19]) is incorrect: they both violate DP and inflate the results.

Contributions. Without a clear understanding of existing methods and an easy-to-use benchmarking platform, it is challenging for the community to make meaningful and reproducible advancements in this field. To bridge this gap, we establish **DPIImageBench**, a benchmark specifically focused on DP image synthesis. **DPIImageBench** addresses the above challenges by making the following contributions:

Taxonomy. We taxonomize methods from two orthogonal dimensions, covering twelve state-of-the-art DP image synthesis algorithms. (1) *Private Data Perspective*. Based on where noise is added to satisfy DP, we categorize methods into (a) *Input-level*: adding noise to (some format of) the sensitive images; (b) *Model-level*: incorporating noise into the gradient or loss during model training; and (c) *Output-level*: introducing noise during the synthesis process. (2) *Public Data Perspective*. Existing works [4], [18] use publicly available data from open platforms without privacy concerns to enhance DP image synthesis. We categorize them into three types based on how the public data is utilized: leveraging pretrained models, public datasets without selection, and public datasets with selection. Besides, we

[†] Co-first author. Kecen is with the Chinese Academy of Science, and this work is done in his personal capacity as a remote intern at UVA.

1. <https://github.com/2019ChenGong/DPIImageBench>.

argue that the state-of-the-art method DP-Promise [24] does not strictly satisfy DP in Appendix E to prevent others from wrongly using it.

Platform. We establish a platform, DPImageBench, with the following contributions: (1) Fair comparison. DPImageBench standardizes the public images, model architectures, and hyper-parameters to ensure fair comparisons. DPImageBench offers an interface to pretrain the synthesizer, even for the ones that were not originally designed to use a public dataset for pretraining. (2) Straightforward implementation. DPImageBench features an abstract interface compatible with any synthesis algorithm. With its modular design, DPImageBench provides a flexible tool that enables users to select public and sensitive datasets, and to integrate new algorithms by adding functional code to the relevant modules. Since DPImageBench isolates the parameter configurations from implementations, users typically only need to modify the configuration files to tune algorithms. (3) Open Source. DPImageBench is open-sourced.¹ It serves as a starting point for the implementation and evaluation of future methods as well.

Evaluation. We have conducted comprehensive evaluations, and some key highlights include: (1) Datasets. DPImageBench implements synthesis methods on **seven** sensitive datasets and **two** public dataset. (2) Fidelity. We establish metrics to assess synthetic images based on similarity, diversity, novelty, and alignment with human perception [25]. (3) Utility. We correct the common evaluation mistakes of using *sensitive test* images for hyper-parameter tuning. Instead, DPImageBench adopts the standard of using distinct training, validation, and test sets for utility evaluations. Downstream classifier training is performed on the training set, hyper-parameter selection is done on the validation set, and final results are reported on the test set. DPImageBench provides two choices of validation set: (1) the synthetic images, and (2) images having the same distribution as the test set but not overlapping with it. In the latter, DPImageBench adds noise to the validation results to satisfy DP, which is detailed in Section 5.3.4.

Insights to new techniques. The proposed taxonomies and straightforward implementations enable us to analyze the potential of combining different methods and bring insight into developing new technology. We consider some methods mostly in isolation, though they can be effectively combined. For example, the public dataset selection method from PrivImage [4] and creating shortcuts for DP training in DP-FETA [26], as described in Section 4, can be paired with other methods. We present details in Section 7.4.

Main findings. From experimental results, we observe several interesting findings, which are described as follows.

- Current methods tend to overestimate the utility of synthetic images. Compared to directly reporting the highest accuracy of classifiers on test sets of the sensitive dataset, (1) using synthetic images as validation sets or (2) adding noise to validation results of the sensitive dataset to ensure DP and avoid bias for classifier tuning, leads to an accuracy decrease of 4.48% and 1.33% under the privacy

TABLE 1: Privacy notion of studied algorithms.

Algorithm	Privacy notion
DP-MERF [28]	Replace-one
DP-NTK [29]	Replace-one
DP-Kernel [17]	Replace-one
PE [5]	Add-or-remove-one
GS-WGAN [15]	Both
DP-GAN [30]	Add-or-remove-one
DPDM [31]	Add-or-remove-one
DP-FETA [26]	Add-or-remove-one
PDP-Diffusion [32]	Add-or-remove-one
DP-LDM [18]	Add-or-remove-one
DP-LoRA [19]	Add-or-remove-one
PrivImage [4]	Add-or-remove-one

budget $\epsilon = 1$, averaged across seven sensitive datasets.

- Current methods using FID [23] and IS [27] are limited in their ability to comprehensively evaluate fidelity. Neither of the metrics considers the novelty or alignment with human perception of synthetic images.
- Pretraining with public datasets does not always benefit DP image synthesis. The effectiveness of pretraining depends heavily on the choice of public dataset and the pertaining strategy (i.e., conditional or unconditional pretraining). Conditional pretraining yields better synthetic performance than unconditional pretraining. A pretraining dataset similar to the sensitive images can enhance synthetic performance.
- The performance of adding noise to low-dimensional features, such as high-level characteristics of sensitive images in DP-MERF [28] and training loss in DP-Kernel [17], is less sensitive to the privacy budget compared to adding noise to high-dimensional features, like weight gradients using DP-SGD. The former methods perform better than the latter under a low privacy budget.
- The combinations of algorithmic improvements, such as integrating DP-FETA [26] into other methods, do not consistently enhance synthetic performance. This inconsistency underscores the need for further research to effectively leverage the strengths of diverse algorithms.

2. Preliminaries

2.1. Privacy Concepts and Mechanisms

DPImageBench concentrates on image synthesis under *differential privacy* (DP) constraint. DP [33] provides mathematical guarantees that quantify and limit the amount of information one can derive from the algorithm’s output and has several properties, including composability [34].

Definition 1 ((ϵ, δ) -DP [33]). *A randomized algorithm \mathcal{A} satisfies (ϵ, δ) -DP if and only if, for any two neighboring datasets D and D' and all possible sets of outputs \mathcal{O} of the mechanism, the following condition holds: $\Pr[\mathcal{A}(D) \in \mathcal{O}] \leq e^\epsilon \Pr[\mathcal{A}(D') \in \mathcal{O}] + \delta$.*

The privacy budget ϵ quantifies how much information can be exposed by the algorithm \mathcal{A} . A smaller value of ϵ implies that the algorithm provides stronger privacy guaran-

tees. The δ can be intuitively understood as failure probability [33]. Given two datasets D and D' , they are considered neighbors (denoted as $D \sim D'$) if we can obtain one from the other by adding, removing, or replacing a single image. We define the ℓ_2 sensitivity (intuitively, a stability measure) of a function f as $\Delta_f = \max_{D \sim D'} |f(D) - f(D')|_2$. As presented in Table 1, two widely used definitions for neighboring datasets exist in existing DP image synthesis: the ‘replace-one’ (bounded DP) and ‘add-or-remove-one’ (unbounded DP) definitions. Specifically, given two datasets D and D' , in the ‘replace-one’ definition, neighboring datasets are defined by *replacing* one image sample, i.e., $D' \cup \{x'\} = D \cup \{x\}$ for image samples x and x' . In the ‘add-or-remove-one’ definition, neighboring datasets are constructed by *adding* or *removing* a single image sample, e.g., $D' = D \cup \{x\}$. We show in Appendix A that all methods that used the replace-one definition can be adapted to add-or-remove-one without affecting their privacy guarantees. As a result, all methods can be compared fairly under the same privacy notion.

Gaussian Mechanism. Gaussian mechanism (GM) adds noise sampled from a Gaussian distribution. For an arbitrary function f with sensitivity Δ_f , the GM \mathcal{A} is defined as,

$$\mathcal{A}(D) = f(D) + \mathcal{N}(0, \Delta_f^2 \sigma^2 \mathbb{I}). \quad (1)$$

$\mathcal{N}(0, \Delta_f^2 \sigma^2 \mathbb{I})$ represents a multi-dimensional random variable drawn from an i.i.d. normal distribution with a mean of 0 and a variance of $\Delta_f^2 \sigma^2$, where σ is a hyper-parameter known as the noise multiplier [33].

DP-SGD. To train machine learning models with DP guarantees, DP-SGD [35] extends standard SGD by controlling the gradient contributions from individual data and applying the Gaussian mechanism. Specifically, in each training iteration, DP-SGD samples a mini-batch from the whole training data D and bounds the sensitivity of each gradient using a clipping operation: $\text{Clip}_C(\mathbf{g}) = \min\left\{1, \frac{C}{\|\mathbf{g}\|_2}\right\} \mathbf{g}$, where \mathbf{g} indicates the original gradient and C is a hyper-parameter. The ‘Clip_C’ operation scales the gradient norm to be at most C , and the model parameters ϕ are then updated using the following equation:

$$\eta \left(\frac{1}{|x|} \sum_{x_i \in x} \text{Clip}_C(\nabla \mathcal{L}(\phi, x_i)) + \mathcal{CN}(0, \sigma^2 \mathbb{I}) \right), \quad (2)$$

where η is the learning rate, \mathcal{L} denotes the loss function of an arbitrary machine learning algorithm, and x refers to a mini-batch sampled from the dataset using Poisson sampling with a rate q (with $|x|$ indicating its size). The $\nabla \mathcal{L}(\theta, x_i)$ denotes the gradient computed for the sample x_i . Besides, $\mathcal{N}(0, \sigma^2 \mathbb{I})$ represents i.i.d. Gaussian noise with variance σ^2 .

As mentioned above, DP-SGD uses only one batch of the sensitive dataset for each iteration of the model parameter update. However, the training process involves many iterations of DP-SGD to ensure that the target model converges. Composition theorems (privacy accounting), e.g., Rényi DP [36], can be used to account for the privacy budget for each iteration and derive the final values of (ϵ, δ) [36].

2.2. Image Generative Models

We introduce three widely used image synthesizers: (1) diffusion models (DMs), including standard DMs [37] and latent DMs [38], (2) Generative Adversarial Networks (GANs) [39], and (3) foundational APIs [5].

Diffusion Models. DMs [37] consist of two processes: (1) The *forward diffusion process* that progressively adds noise to a clean image x_0 until it becomes close enough to pure random noise, generating a sequence of increasingly noisy images $\{x_i\}_{i=1}^T$, where T is the number of noising steps. (2) The *reverse process* that progressively denoises a random noise to a clean image via a trainable neural network. In the forward diffusion process, the transition between adjacent noisy images, $p(x_t | x_{t-1})$, follows a multi-dimensional Gaussian distribution,

$$p(x_t | x_{t-1}) = \mathcal{N}\left(x_t; \sqrt{1 - \beta_t} x_{t-1}, \beta_t \mathbb{I}\right)$$

where β_t is a hyper-parameter that defines the variance of the noise distribution at each step. We denote $\bar{\alpha}_t = \prod_{s=1}^t (1 - \beta_s)$. The likelihood between the clean image x_0 and its noisier version at step t is derived as, $p(x_t | x_0) = \mathcal{N}(x_t; \sqrt{\bar{\alpha}_t} x_0, (1 - \bar{\alpha}_t) \mathbb{I})$. Then, we can sample x_t directly from x_0 in closed form,

$$x_t = \sqrt{\bar{\alpha}_t} x_0 + e_t \sqrt{1 - \bar{\alpha}_t}, e_t \sim \mathcal{N}(0, \mathbb{I}) \quad (3)$$

The final objective of DMs is to train a network to predict the added noise at each step, as defined in [37].

$$\mathcal{L} = \mathbb{E}_{x_0 \sim D, t \sim \mathcal{U}(1, T), e_t \sim \mathcal{N}(0, \mathbb{I})} \|e - e_\theta(x_t, t)\|^2 \quad (4)$$

where D is the dataset of clean images and e_θ is a denoising network parameterized by θ . The network $e_\theta(x_t, t)$ learns to predict the noise e in any noisy image x_t at step t . Once well-trained, e_θ can be used to denoise random Gaussian noise into a clean image.

Latent Diffusion Models (LDMs). LDMs [38] are a variant of DMs that operate in a latent space instead of directly in pixel space. LDMs first use a pretrained autoencoder to map images into a lower-dimensional latent representation. The same diffusion and denoising steps discussed before proceed in this compressed latent space rather than on raw pixels. After performing the reverse diffusion steps in latent spaces, the decoder reconstructs final high-resolution images. LDMs operate in a lower-dimensional space, enabling more efficient training and sampling than standard pixel-based DM.

Stable diffusion is a representative example of LDMs that generate images from textual descriptions or class labels. DP-LDM [18] and DP-LoRA [19] leverage stable diffusion [38] as the synthesizer.

Generative Adversarial Nets (GAN). GAN consists of two networks: a generator Gen and a discriminator Dis [39], [40]. The generator Gen receives a random noise vector and outputs an image. The discriminator Dis receives an image and outputs a score, which indicates how real the input image is. The Gen is trained to deceive the discriminator, and the Dis is trained to distinguish whether its input image comes from the true dataset or is generated by the Gen. Both

networks are trained simultaneously, constantly improving in response to each other’s updates. Overall, the objective function of GAN is defined as,

$$\min_{\text{Gen}} \max_{\text{Dis}} V(\text{Gen}, \text{Dis}) = \mathbb{E}_{x \sim q(x)} [\log \text{Dis}(x)] + \mathbb{E}_{z \sim p(z)} [\log (1 - \text{Dis}(\text{Gen}(z)))] \quad (5)$$

The $q(x)$ and $p(z)$ indicate the distributions of the real image and noise vector. After the training is done, the discriminator is discarded, and the generator can be used for generation.

Foundational APIs. Foundation APIs are either cloud-based services (e.g., Dall-E [41]) or local software libraries (e.g., Stable Diffusion [38]) that provide simple API access to powerful, pretrained models capable of generating high-quality synthetic images. The underlying model can be any generative model, including diffusion models and GANs.

2.3. DP Image Synthesis

Various sensitive image datasets, such as medical images [42] and face images [43], face the risk of privacy leakage. Attackers may infer information about the training dataset from the synthetic images [44]. DP image synthesis aims to generate artificial images that closely resemble real data while ensuring the privacy protection of the original dataset. DP quantifies leakage to infer the training dataset using the synthetic dataset. These methods enable organizations to share and use synthetic images for various downstream analyses, reducing privacy concerns. We introduce current state-of-the-art DP image synthesis methods and present their taxonomy in Section 4.

3. Overview of DPImageBench

We introduce DPImageBench, a modular toolkit designed to evaluate the performance of DP image synthesis algorithms in terms of utility and fidelity. We envisage DPImageBench for the following four purposes.

- DPImageBench should incorporate advanced synthesis methods that are widely used and have achieved state-of-the-art performance within the community.
- This benchmark should enable users to apply these techniques to their own private image datasets as well as public datasets for DP image release.
- We intend for DPImageBench to offer straightforward implementation methods and consistent hyper-parameter settings for the studied methods, facilitating a comprehensive understanding of their strengths and weaknesses.
- DPImageBench should comprehensively evaluate the quality of synthetic images generated by different algorithms for comparative studies.

As presented in Figure 1, we design four key modules for DPImageBench, to achieve these goals point by point: **(1) Model Selection.** DPImageBench allows users to select among twelve distinct DP image synthesis algorithms, which are categorized into three groups as introduced in Section 4. DPImageBench also provides simple interfaces to allow users to integrate new algorithms.

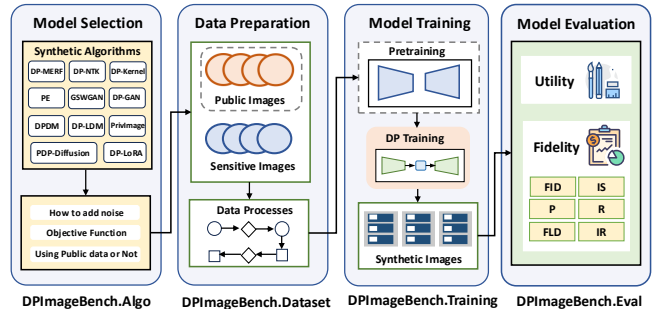


Figure 1: Overview of DPImageBench. The operations in the gray dashed box mean using public images for pretraining, which is optional, depending on the algorithms.

(2) Data Preparation. This module prepares the public images and sensitive images for the following modules by partitioning and preprocessing the data, such as normalization. DPImageBench offers a flexible tool that allows users to select public and sensitive datasets.

(3) Model Training. This module involves (optional) synthesizer pretraining on the public dataset and the main training on the sensitive dataset. We unify the model architectures and hyper-parameters across different methods. Besides, we provide flexible configuration files, allowing users to adjust hyper-parameters according to their preferences. DPImageBench supports pretraining for all algorithms, even those not originally designed with pretraining. Details of the pretraining methods are provided in Appendix B.2.3.

(4) Evaluation. This module assesses the synthetic images generated by algorithms on aspects of utility and fidelity.

In the following section, we elaborate on the taxonomy method for model selection in Section 4, followed by the key design elements of DPImageBench for data preparation, model training, and evaluation in Section 5.

4. Taxonomy and Method Description

This section provides an overview of the taxonomy and elaborates on DP image synthesis algorithms. We present a novel taxonomy of existing methods from two orthogonal dimensions: (1) The Private Data Perspective: where the noise is added, and (2) The Public Data Perspective: how public data is used to enhance DP image synthesis. Note that this paper does not intend to benchmark every possible method but focuses only on state-of-the-art ones. For example, we omitted some GAN- and VAE-based methods, which are not state-of-the-art [4], [18], [31]. Additionally, we include all diffusion-based algorithms due to their exceptional performance. That said, as DPImageBench is a general framework, users can always add more methods to it.

4.1. The Private Data Perspective

We formulate the pipeline of DP image synthesis as follows: public images and sensitive images are fed into the synthesizer for pretraining and finetuning. The well-trained models then generate synthetic images as output. We propose a taxonomy based on where noise is added, as

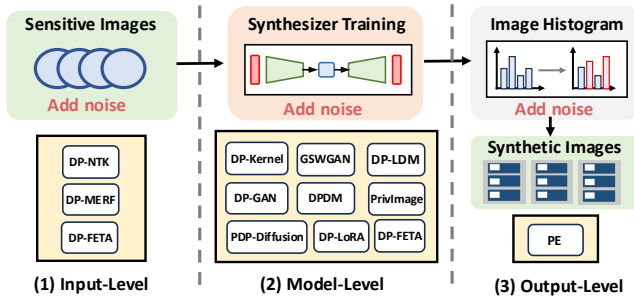


Figure 2: The private data perspective in taxonomy categorizes the studied algorithms into three levels: input-level, model-level, and output-level.

outlined in Table 1, categorizing current methods into input-level, model-level, and output-level approaches (Figure 2).

- *Input-level*: DP-MERF and DP-NTK add noise to the feature embeddings of sensitive images.
- *Model-level*: GS-WGAN, DP-LDM, DP-GAN, DPDM, PrivImage, and PDP-Diffusion use DP-SGD to train the synthesizer on sensitive images while ensuring DP. DP-Kernel adds noise to the training loss of the synthesizer.
- *Output-level*: PE leverages model inference APIs to generate images and uses each private image to iteratively vote for the most similar API-generated images, forming a voting histogram. Noise is added to this histogram for DP, guiding pretrained models to generate images.
- *Mix-level*: Our taxonomy enables the systematic analysis of algorithms that introduce noise at various levels, such as DP-FETA, which applies noise at both the input and model levels.

This taxonomy also reveals the potential of combining privacy sanitization methods across various levels. For example, the finetuning-free method, PE, heavily relies on the pretrained model’s ability to generate images similar to the sensitive ones. Its performance may be suboptimal if the model fails in this regard. Our taxonomy offers a clear framework that can guide PE in incorporating finetuning on sensitive images to enhance performance.

We explain in Appendix E why the state-of-the-art method DP-Promise [24] does not strictly satisfy DP and, therefore, is not included in our analysis.

4.1.1. Input-Level. These algorithms first extract high-level statistical characteristics from images. They then add noise to these characteristics to ensure privacy.

DP-MERF [28]. This method uses random Fourier feature representations [45] of Gaussian kernel mean embeddings as the high-level statistical characteristics of the image dataset. Kernel mean embedding (KME) [46] maps a probability distribution into a reproducing kernel Hilbert space (RKHS) [47] by computing the mean of kernel evaluations. DP-MERF uses random Fourier features to approximate KME. Under DP constraints, DP-MERF adds noise, determined by the Gaussian mechanism [36], to the KME of sensitive images. Then, DP-MERF trains a generator that minimizes the Maximum Mean Discrepancy (MMD) [48] between the noisy KME and the KME of the generated images.

DP-NTK [29]. This method claimed that directly computing the KME from the original image dataset is challenging due to the high dimensionality of the images [29], [49]. They propose the use of Neural Tangent Kernels (NTKs) [50], which provide an improvement over the Gaussian kernel used in DP-MERF [28]. In particular, DP-NTK introduces the NTK to represent images, whereby the gradient of the neural network function acts as the feature map to extract perceptual features from the original images. Computing KME based on these perceptual features extracted from NTKs yields improved synthetic image quality.

4.1.2. Model-Level. These methods add DP noise in the training stage of generative models.

DP-Kernel [17]. DP-MERF matches the KME across all data, which can lead to *mode collapse* [51], resulting in synthetic images that are overly similar. Besides, using random Fourier features to approximate KME may also cause potential errors. Instead of adding Gaussian noise to the KME of sensitive images in DP-MERF, DP-Kernel proposes directly adding noise to the MMD loss function that measures the discrepancy between the distributions of sensitive and synthetic images in an RKHS to avoid the mentioned issues.

$$\tilde{\mathcal{L}}_{\text{MMD}}(p, q) = \mathcal{L}_{\text{MMD}}(p, q) + \text{Gaussian noise},$$

where p and q represent the distribution of real and synthetic images by the generator.

DP-GAN [30]. As described in Section 2.2, the discriminator in GANs guides the generator to generate images similar to the real images. DP-GAN trains the discriminator network on the sensitive images using DP-SGD, ensuring that the discriminator weights satisfy DP. As presented in Eq. (5), the weight update of the generator solely relies on the discriminator. Due to the post-processing property of DP [52], the generator also satisfies DP.

DPDM [31]. This paper is the first to use DMs [37] as the DP synthesizer. It trains DMs on sensitive images using DP-SGD to ensure DP. Traditional DMs without DP often use small batch sizes and heavily over-parameterized architectures [37], [53]. Under DP, these factors can result in high levels of noise [35], which affects the performance of synthesis. DPDM introduces modifications to DP-SGD specifically tailored for the DP training of DMs to alleviate this issue. In particular, DPDM introduces the *noise multiplicity*, where the image is re-used for training to learn to denoise at multiple steps. DPDM shows that this modification does not incur additional privacy cost, while reducing the variance of the diffusion training objective.

GS-WGAN [15]. Unlike DPGAN, which applies perturbations to the entire discriminator, GS-WGAN perturbs only the feedback from the discriminator that guides the generator’s training, thereby ensuring DP in synthesizing images. Specifically, GS-WGAN decomposes the generator’s gradient into two components using the chain rule: an *upstream gradient* (the output of discriminator with respect to the generated image) and a *local gradient* (the generated image with respect to the generator’s parameters). The

upstream gradient is perturbed using GM to satisfy DP, as only the discriminator has direct access to sensitive images during training. By building a “privacy barrier” between the discriminator and the generator, this approach ensures that private information does not leak into the generator. This property allows GS-WGAN to pretrain the discriminators of GAN on sensitive images without considering privacy to warm up the synthesizing.

PDP-Diffusion [32]. This paper first proposes the paradigm of pretraining the DP image synthesizer on a public dataset without privacy concerns. By leveraging this public dataset, the synthesizer can benefit from a broader knowledge base, which may enhance its performance during the subsequent DP-SGD [35] finetuning process on the sensitive dataset. Later methods using DMs, such as DP-LDM [18] and PrivImage [4], are all built upon this paradigm.

DP-LDM [18]. DP-LDM [18] proposes using LDMs as synthesizers instead of standard DMs used in previous works [32]. It further improves efficiency by finetuning only specific components of the pretrained LDM, namely the label embedding module [38] and the attention module [54]. DP-LDM reduces the number of trainable parameters and requires less noise to maintain the same privacy budget.

DP-LoRA [19]. Built on DP-LDM, DP-LoRA uses Low-Rank Adapters (LoRA) [55], a parameter-efficient finetuning approach, to train LDMs, thus reducing the size of trainable parameters and improving the privacy-utility trade-off.

PrivImage [4]. This paper highlights that a dataset with a distribution similar to the sensitive dataset is more suitable for pertaining [11], [13]. This insight motivates PrivImage to select pretraining data with a distribution that closely matches the sensitive dataset. PrivImage proposes to describe the distribution of image datasets using semantics [56]. Unlike focusing on the low-level features such as color, texture, and edges that can be directly extracted from an image, semantics provides a high-level understanding of images, including their “meaning” or “content” [56].

To access the semantic distribution of images, PrivImage first establishes a semantic query function using the public dataset D_p . This function can be an image captioning method [57], [58] or an image classifier. The objective of query function is defined as [4]:

$$\mathcal{L}_Q = \mathbb{E}_{(x,s) \sim D_p} \left[\sum_{i=1}^{NS} - (s_i \log Q_i(x)) \right].$$

Here, D_p represents the public dataset, where each entry consists of an image x and its associated semantic labels s . NS denotes the number of possible semantic labels in D_p . A label $s_i = 1$ indicates that the image possesses the i -th semantic label, while $s_i = 0$ signifies its absence. The function $Q_i(x)$ represents the probability that image x has semantic s_i . PrivImage extracts semantics from sensitive images using a query function, adds Gaussian noise to the queried semantic distribution to ensure DP, and then selects a subset of public images for pretraining based on this noisy distribution. Finally, PrivImage pretrains the synthesizer on the selected dataset and then fine-tunes the model on the sensitive dataset using DP-SGD [35].

TABLE 2: Overview and comparison of studied algorithms. “✓” indicates that the algorithm involves this property, while “✗” indicates that it does not.

Algorithm	Pretrain	Privacy		Model Type
		Type	Noise Added	
DP-MERF	✗	Input	Feature Embedding	GAN
DP-NTK	✗	Input	Feature Embedding	GAN
DP-Kernel	✗	Model	Training Loss	GAN
PE	✓	Output	Histogram	API
GS-WGAN	✗	Model	Output Gradient	GAN
DP-GAN	✗	Model	Weight Gradient	GAN
DPDM	✗	Model	Weight Gradient	DM
DP-FETA	✗	Mix	Weight Gradient & Images	DM
PDP-Diffusion	✓	Model	Weight Gradient	DM
DP-LDM	✓	Model	Weight Gradient	LDM
DP-LoRA	✓	Model	Weight Gradient	LDM
PrivImage	✓	Model	Weight Gradient	DM

4.1.3. Output-Level. These papers introduce noise during the synthesis process to assist in selecting synthetic images that are most similar to the sensitive images under DP.

Private Evolution (PE) [5]. This method uses the foundation APIs, which can come from either blackbox API-based models such as DALLE-2 [41] or open-sourced models like Stable Diffusion [38]. PE iteratively uses each private image to vote for the most similar images generated by the APIs, forming a voting histogram. DP is ensured by adding noise to this histogram. Using the noisy histogram, PE identifies the images most similar to the private ones and then prompts the pretrained models to generate more variations of them. As a result, PE can be applied to any generative model capable of producing variations of an image (such as diffusion models by adding noise to the image and using the model to denoise it). Notably, PE relies solely on model inference and does not require any training on sensitive images. Lin et al. [5] prove that the distribution of images generated by PE can converge to that of the private images.

4.1.4. Mix-Level. This taxonomy facilitates the analysis of methods that apply DP noise at multiple levels.

DP-FETA [26]. This method enables synthesizers to learn image features progressively from simple to complex. DP-FETA divides the training process for generating complex images into two stages: (1) DP-FETA extracts basic features, such as rough outlines and colors, from sensitive images using “central images”—representations of central tendency measures (e.g., mean, mode). These images, perturbed with Gaussian noise at the “input level” to ensure DP, build a shortcut to facilitate early-phase synthesizer training. After the training on central images, the diffusion models can generate rough and statistically imperfect images. (2) The synthesizer is then fine-tuned on original sensitive images using DP-SGD [35] to generate more realistic images, with noise added at the “model-level.”

4.2. The Public Data Perspective

As shown in Table 2, pretraining synthesizers on public datasets, such as ImageNet [59], which are openly available and do not raise privacy concerns, can enhance the utility and fidelity of DP synthetic images [4], [18], [32]. We believe that pretraining brings new insight into the

community. Previous taxonomy lacks a systematic analysis of how public data is utilized [1], [20]. We fill this gap and outline potential directions as follows.

- *Pretrained model*: PE [5] utilizes inference APIs of foundation models, which have been trained on public datasets.
- *Public dataset without selection*: DP-LDM and PDP-Diffusion use the whole public dataset for pretraining.
- *Public dataset with selection*: PrivImage [4] shows that selecting a subset of pretraining images whose distribution closely matches the sensitive dataset yields better performance compared to using the entire public dataset.

This taxonomy provides insights for developing new technologies. (1) Inspired by the public dataset selection approach in PrivImage, one potential avenue is to refine methods that do not consider selecting pretrained models (like PE). (2) Integrating the public dataset selection into approaches that have not yet been considered could be another promising direction. Specifically, in Section 7.3, we investigate how incorporating the public dataset selection approach from PrivImage into methods without selection can enhance synthetic performance.

5. Key Designs of DPImageBench

5.1. Data Preparation

DPImageBench offers a flexible tool that allows users to select both public and sensitive datasets. This setup facilitates the pretraining of DP image synthesizers on public datasets for all studied algorithms, including those that were not initially designed to leverage public datasets for pretraining, e.g., DP-MERF [28], DP-NTK [29], etc. The `README.md` file of our repository¹ provides instructions for users to customize their dataset.

5.2. Model Training

5.2.1. The Failure Probability δ . For a meaningful DP guarantee, δ should satisfy that $\delta \ll \frac{1}{N}$, where N presents the size of the sensitive dataset [60]. Many previous works ignore this relationship and use $\delta = 1 \times 10^{-5}$. In DPImageBench, we set $\delta = 1/N \log(N)$ following prior works [9], [60].

5.2.2. Unified Framework. Failing to standardize the pretraining dataset and model architectures can result in unfair comparisons. Even when the same model type is used as the synthesizer, variations in the hyper-parameters of the synthesizer and DP-SGD (e.g., batch sizes, epochs, and learning rates) can greatly influence performance. DPImageBench standardizes the public images for pretraining and model architectures to ensure fair and consistent comparisons.

In DP-LDM and DP-LoRA, the synthesizer uses stable diffusion [38]. In contrast, other methods, such as DPDM [31] and PrivImage [4], rely on standard DMs. As described in Section 2.2, LDMs are implemented by incorporating an autoencoder into DMs. Therefore, DPImageBench provides standardized implementations for the common components of both LDMs and standard DMs,

TABLE 3: Overview of evaluations for the studied algorithms. “ ϵ (min, max)” mean the minimum and maximum values of ϵ used for DP image synthesis in their paper.

Algorithm	Fidelity	Utility	DP testing	ϵ (min, max)
DP-MERF [28]	✗	Acc	✗	(0.2, 10.0)
DP-NTK [29]	✗	Acc	✗	(0.2, 10.0)
DP-Kernel [17]	FID	Acc	✗	(0.2, 1.0)
PE [5]	FID	Acc	Nearest Sample	(0.1, 32.0)
GS-WGAN [15]	FID, IS	Acc	✗	(0.1, 85.0)
DP-GAN [30]	FID	Acc	✗	(9.6, 29.0)
DPDM [31]	FID	Acc	✗	(0.2, 10.0)
DP-FETA [26]	FID	Acc	✗	(1.0, 10.0)
PDP-Diffusion [32]	FID	Acc	✗	(10.0, 10.0)
DP-LDM [18]	FID	Acc	✗	(1.0, 10.0)
DP-LoRA [19]	FID	Acc	✗	(0.2, 10.0)
DP-Promise [24]	FID, IS	Acc	✗	(1.0, 10.0)
PrivImage [4]	FID	Acc	MIA	(1.0, 10.0)

including the structure of the noise prediction network and hyper-parameters of DP-SGD. We also implement DP-LDM with *standard* DMs to examine the extent to which performance improvements are influenced by differences in the synthesizer architecture. We refer to the DP-LDM that applies standard DMs as “DP-LDM (SD).”

5.2.3. Extensions to New Algorithms. DPImageBench has a modular design to make it easy to (1) add new algorithms and (2) develop new algorithms based on refining current methods (e.g., PDP-Diffusion and PrivImage are both built based on DPDM).

To add new algorithms, users simply need to implement the abstract base class with three interfaces: (1) pertaining the synthesizer with a public image dataset as input, (2) training the synthesizer with a sensitive image dataset as input, and (3) generating synthetic images. Users can flexibly design their methods inside the interfaces.

To refine existing methods, since DPImageBench isolates the parameter configurations from the algorithm implementation, users typically only need to modify the configuration files to adjust hyperparameters and refine algorithms.

We provide examples in the `README.md` file of our repository¹ to illustrate how to add new algorithms.

5.3. Evaluation

After the evaluation is done, the results, including the synthetic images, logs, and metrics, are stored in the ‘exp’ folder. Please see the `README.md` file of our repository¹ for more detail.

5.3.1. Previous Synthesis Evaluations. Table 3 summarizes the evaluations of the investigated algorithms. We introduce them as follows.

Fidelity. The Fréchet Inception Distance (FID) [23] evaluates the quality and diversity of generated images by measuring the distance between the feature distributions of sensitive and synthetic images within the feature space of a pretrained network. It is used by all papers. Inception Score (IS) [27] evaluates the generated images by assessing how confidently the images are classified and how diverse they are across different classes (mode coverage) [61]. Note that

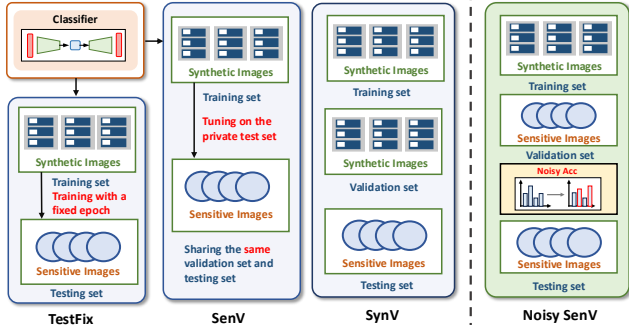


Figure 3: Comparison between current utility evaluation methods and our proposed approach.

IS only makes sense for natural images (e.g., the ones in the ImageNet dataset [59]).

Utility. Utility considers how synthetic images perform in downstream analytics. The most widely explored task is classification. In particular, current studies train classifiers on synthetic images and evaluate the classification accuracy (Acc) using sensitive test datasets.

Empirical DP testing. Current DP image synthesis methods [4], [5], [22] propose to empirically estimate the privacy leakage from the synthetic images under DP constraints. In PrivImage, authors leverage MIAs [44] to infer the sensitive images for the synthetic images. Lin et al. [5] compared the distribution of distances between synthetic images and their nearest sensitive images to confirm that the synthetic images are not copies of private images.

5.3.2. Fidelity Evaluations. As discussed above, most DP image synthesis methods evaluate the fidelity of synthetic images using the FID [23] and IS [27]. They have certain limitations, such as being insensitive to whether synthetic images memorize training images and lacking alignment with human perception [61]. We establish evaluation from four perspectives.

- *Similarity.* Evaluates the proportion of synthetic images that resemble images in the real dataset.
- *Diversity.* Assesses the variety in images to ensure the generated data covers the full range of the real dataset.
- *Novelty.* Evaluates how distinct the synthetic images are from the images in the training dataset, focusing on avoiding overfitting or memorization.
- *Human.* Incorporates human perception to assess the realism of synthetic images from a subjective standpoint.

DPIImageBench introduces precision and recall [62], which provide separate scores to offer a clearer understanding of whether a model excels at generating high-quality images (precision) or diverse images (recall). Moreover, DPIImageBench also incorporates Feature Likelihood Divergence (FLD) [61], which evaluates the novelty of the synthetic dataset. From a human-level perspective, we introduce additional evaluation metrics ImageReward (IR) [25]. We briefly outline the selected metrics as follows:

FID: FID [23] first uses Inception-v3 [63] to extract features from synthetic and sensitive images. It estimates multivariate

TABLE 4: Overview of utility evaluations for the studied algorithms. “X” indicates that it did not release codes.

Algorithm	Evaluation Way	Algorithm	Evaluation Way
DP-MERF	Test on a fixed epoch	DPDM	Synthetic images as val
DP-NTK	Test on a fixed epoch	PDP-Diffusion	X
DP-Kernel	Test on a fixed epoch	DP-LDM	Synthetic images as val
PE	Sensitive test set as val	DP-LoRA	Sensitive test set as val
GS-WGAN	Sensitive test set as val	DP-FETA	Sensitive test set as val
DP-GAN	X	PrivImage	Sensitive test set as val

Gaussian distributions from these features and calculates the FID score by measuring the Fréchet distance [23] between the two distributions. A lower FID indicates that the generated images are more similar to the real dataset.

IS: The IS uses the Inception v3 [63] network to classify each generated image into predefined classes. A higher IS indicates that the synthetic images are both realistic (the model classifies them with high confidence) and diverse (the images span various classes).

Precision and Recall: We begin by extracting features from both sensitive and synthetic images using the Inception v3. Next, for each synthetic image, we identify the closest sensitive image in the feature space. If the distance between the synthetic image and the sensitive image falls below a specified threshold, we classify it as a “true positive.” Precision is then calculated as $\frac{\text{Number of True Positives}}{\text{Total Generated Images}}$. Additionally, for recall, we locate the nearest synthetic image for each sensitive image. Here, a “True Positive” is defined as a pair where the distance between the images is below the threshold, and Recall is calculated as $\frac{\text{Number of True Positives}}{\text{Total Real Images}}$. Achieving higher Precision and Recall is preferable, although there is often a trade-off between them [62].

FLD: We refer to the repository released by Jiralerspong et al. [61]. A lower FLD value is better, with negative values indicating the synthetic dataset outperforms the original.

IR: IR is the state-of-the-art method for assessing synthetic images from a human perspective. We use the image labels as the text description. A higher IR value indicates that the synthetic images align more with human preferences.

5.3.3. Utility Evaluations. When evaluating synthetic image utility, many studies use simple classifiers, limiting classification performance and reducing evaluation credibility. For instance, DP-MERF [24] reports the best accuracy of 87.9% on real FashionMNIST dataset, which is lower than the 94.4% achieved by Inception v3 [63]. DPIImageBench trains classifiers using methods that achieve accuracy comparable to SOTA methods. We also provide options for the other classification algorithms.

5.3.4. Promoting Utility Evaluations. Current utility evaluation methods exhibit drawbacks. As described in Table 4, previous works consider three explicit ways to evaluate utility: (1) *Test on a fixed epoch* (TestFix): Train the classifier up to a predetermined epoch, then directly evaluate it on the sensitive test set. (2) *Sensitive test set as val* (SenV): Train classifiers on the synthetic images, and use test sets without separate validation sets for *tuning* classifier to select optimal parameters. (3) *Synthetic images as val* (SynV): Use the synthetic images as the validation set for classifier selection.

TABLE 5: Summary of investigated datasets used for evaluation. Images from the ImageNet dataset have varying dimensions but are typically resized to 256×256 for generation tasks.

Dataset	Size	Dimension	Category	Training	Validation	Test	Task	Effect
MNIST [64]	70,000	$28 \times 28 \times 1$	10	55,000	5,000	10,000	Classification	Sensitive
FashionMNIST [65]	70,000	$28 \times 28 \times 1$	10	55,000	5,000	10,000	Classification	
CIFAR-10 [66]	60,000	$32 \times 32 \times 3$	10	45,000	5,000	10,000	Classification	
CIFAR-100 [66]	60,000	$32 \times 32 \times 3$	100	45,000	5,000	10,000	Classification	
EuroSAT [67]	27,000	$64 \times 64 \times 3$	10	21,000	2,000	4,000	Classification	
CelebA [43]	182,732	$128 \times 128 \times 3$	2	145,064	17,706	19,962	Classification	
Camelyon [42]	337,340	$64 \times 64 \times 3$	2	269,538	32,898	34,904	Classification	
ImageNet ISLVR2012 [59]	1,431,167	$256 \times 256 \times 3$	1,000	1,281,167	50,000	100,000	Pretraining	Public
Places365 [68]	2,141,660	$256 \times 256 \times 3$	365	1,803,460	17,800	320,400	Pretraining	

TABLE 6: Comparison of the utility evaluations. “✓” indicates that the method involves this property, while “✗” indicates that it does not.

Methods	Tuning for Better Results	Avoid Bias	Satisfy DP
TestFix	✗	✗	✓
SenV	✓	✗	✗
SynV	✓	✓	✓
Noisy SenV (Ours)	✓	✓	✓

As presented in Table 6, previous works both have drawbacks as follows,

- **TestFix**: The optimal classifier training iterations that do not cause overfitting and underfitting depend on the data. ‘TestFix’ trains classifiers for a predetermined number of epochs, which is not necessarily optimal.
- **SenV**: Even worse, as Figure 3 illustrates, ‘SenV’ leads to two key issues: (1) *Bias in Test Accuracy*: Using the Test set for model selection biases results in higher accuracy. (2) *Privacy Risks*: Model selection based on test or validation metrics from sensitive datasets may breach DP guarantees [69], as the test and validation sets share distributions with the training data.
- **SynV**: Due to the distribution gap between synthetic images and sensitive images, using synthetic images as the validation set to select classifiers for the sensitive set may underestimate the utility.

DPIImageBench presents the solutions to overcome the three issues presented in Table 6 as follows.

To address the tuning and the bias issues, Figure 3 illustrates that we use the sensitive validation set (as detailed in Table 5), which is distinct from the sensitive training and test set, for classifier tuning. However, the validation set shares the same distribution as the sensitive training data, potentially still violating DP [69].

To satisfy DP, we use the “report noisy max” method [70]. We select the best classifier checkpoint that has the most correct samples. To satisfy ϵ -DP, we add the Laplace noise from $\text{Lap}(1/\epsilon)$ to their correct number and select the best classifier checkpoint based on the noisy numbers. The best classifier is used to calculate the test set accuracy. Since the training and validation sets are two disjoint sets, according to the *parallel composition theorem* [71], the ultimate privacy guarantee depends only on the worst of the guarantees of each analysis, $\max\{\epsilon_t, \epsilon_v\}$, where ϵ_v is the privacy costs of the validation set and ϵ_t is the privacy cost of training the synthesizer on the training set.

DPIImageBench sets $\epsilon_t = \epsilon_v$ without additional privacy cost. Thus, the final privacy cost is still ϵ_t [52]. We abbreviate this method as ‘Noisy SenV’.

In DPIImageBench, we provide ‘SynV’ and ‘Noisy SenV’, the two methods that satisfy DP, avoid bias, and support tuning, as the utility evaluation metrics.

5.3.5. Empirical DP Testing. Empirical DP testing is an experimental approach to auditing the privacy properties of an algorithm. This method involves running the algorithm with specially constructed data to empirically assess DP parameters and/or measure the potential exposure of personal information in the input data. The goal is to determine whether the system effectively obscures sensitive details and adheres to the privacy standards of the DP [72].

We chose not to perform empirical DP testing for the following reasons. (1) *Lack of suitable methods*: Most existing research focuses on auditing DP in *classification* models [72], [73], models trained on non-image data (e.g., tabular data [74]), or the DP-SGD algorithm [75], [76]. Applying these methods to our problem is not straightforward, as we focus on DP *image generation*, and some of the approaches we evaluate, such as PE, do not use DP-SGD. (2) *Theoretical guarantee*: DP synthesis algorithms already have the rigorous theoretical privacy guarantee that the sensitive information leaked from the output data is bounded. If the goal is empirical privacy, we do not even need DP in the first place.

That said, we believe empirical DP testing is still an important direction that can flag the errors of DP implementation. We call for future research on DP auditing for *image synthesis*.

6. Experimental Setup

Appendices B.1 and B.2.1 introduce algorithm implementations and hyper-parameter settings. Appendix B.2.6 discusses privacy costs for hyper-parameter tuning.

6.1. Investigated Datasets

Referring to previous works [4], [5], [24], [31], [32], we assume that the investigated datasets can be divided into *sensitive datasets* that require protection and *public datasets* that can be released publicly without privacy concerns.

TABLE 9: Fidelity evaluations of synthetic images under $\epsilon = 10$ and $\delta = 1/N \log(N)$, where N is the size of the sensitive dataset. Due to the space limitation, we report the results of the Camelyon dataset in Table 18 of the Appendix. Note that IS is more informative in natural image datasets such as CIFAR-10 and CIFAR-100; we include it in all datasets for completeness.

Algorithm	MNIST						FashionMNIST						CIFAR-10					
	FID↓	IS↑	Precision↑	Recall↑	FLD↓	IR↑	FID↓	IS↑	Precision↑	Recall↑	FLD↓	IR↑	FID↓	IS↑	Precision↑	Recall↑	FLD↓	IR↑
DP-MERF	106.3	2.64	0.03	0.03	34.9	-2.23	106.4	2.86	0.08	0.01	29.2	-2.05	214.1	3.06	0.25	0.00	32.1	-2.27
DP-NTK	69.2	2.18	0.09	0.08	25.5	-2.21	120.5	3.05	0.04	0.00	36.4	-2.19	346.9	1.59	0.01	0.00	41.7	-2.27
DP-Kernel	38.9	2.19	0.24	0.02	17.8	-2.18	74.2	3.45	0.23	0.01	21.3	-1.95	161.4	3.69	0.18	0.00	27.2	-2.27
PE	45.3	2.79	0.08	0.28	25.6	-2.21	23.1	5.37	0.15	0.53	16.1	-1.90	9.2	14.97	0.59	0.54	2.7	-1.31
GS-WGAN	47.7	2.37	0.13	0.01	25.4	-2.14	97.2	2.95	0.17	0.00	28.1	-1.95	194.4	2.34	0.17	0.00	31.1	-2.28
DP-GAN	30.3	2.06	0.19	0.22	15.0	-2.16	76.9	3.60	0.17	0.02	23.9	-1.94	138.7	2.65	0.67	0.01	22.5	-2.28
DPDM	4.4	2.07	0.63	0.73	3.3	-2.00	17.1	3.92	0.54	0.38	6.6	-1.63	110.1	3.12	0.59	0.04	19.4	-2.21
DP-FETA	3.4	2.09	0.66	0.77	2.7	-1.99	13.2	3.93	0.60	0.43	4.6	-1.61	114.0	3.30	0.63	0.02	18.6	-2.22
PDP-Diffusion	3.8	2.87	0.61	0.82	3.4	-2.02	6.2	4.23	0.53	0.71	4.9	-1.66	18.4	8.11	0.50	0.66	7.2	-2.09
DP-LDM (SD)	18.7	2.23	0.21	0.77	12.2	-2.13	20.1	4.33	0.32	0.71	11.7	-1.87	19.8	8.14	0.48	0.68	9.0	-2.13
DP-LDM	99.1	1.85	0.00	0.03	32.1	-2.18	53.2	3.74	0.28	0.40	15.4	-1.87	47.4	6.40	0.49	0.49	14.1	-2.23
DP-LoRA	95.4	1.85	0.00	0.03	32.1	-2.18	43.7	3.98	0.26	0.53	14.8	-1.89	27.8	7.64	0.49	0.64	9.3	-2.18
PrivImage	2.3	2.16	0.62	0.83	2.8	-2.01	5.3	4.29	0.56	0.72	4.3	-1.64	13.1	8.41	0.56	0.63	5.1	-1.92

Algorithm	CIFAR-100						EuroSAT						CelebA					
	FID↓	IS↑	Precision↑	Recall↑	FLD↓	IR↑	FID↓	IS↑	Precision↑	Recall↑	FLD↓	IR↑	FID↓	IS↑	Precision↑	Recall↑	FLD↓	IR↑
DP-MERF	197.5	2.93	0.32	0.00	25.2	-2.26	182.2	2.20	0.05	0.00	34.6	-2.26	147.9	3.61	0.08	0.00	17.1	-2.20
DP-NTK	398.1	1.28	0.13	0.00	43.0	-2.28	257.6	1.95	0.06	0.00	40.3	-2.27	227.8	3.21	0.05	0.00	30.6	-2.23
DP-Kernel	224.1	2.43	0.12	0.00	26.1	-2.27	181.6	2.52	0.05	0.01	32.2	-2.23	128.8	2.90	0.11	0.00	14.4	-1.72
PE	9.6	19.65	0.58	0.54	3.7	-2.22	48.1	8.16	0.08	0.69	16.7	-2.10	22.0	3.87	0.28	0.52	5.1	-0.96
GS-WGAN	246.4	1.87	0.44	0.00	26.1	-2.28	236.3	1.75	0.02	0.0	45.0	-2.28	290.0	1.66	0.03	0.00	43.2	-2.27
DP-GAN	181.0	2.34	0.45	0.00	23.2	-2.28	222.4	1.95	0.03	0.00	47.0	-2.27	31.7	2.28	0.62	0.05	3.9	-0.69
DPDM	130.2	2.73	0.68	0.01	19.0	-2.23	168.8	1.67	0.61	0.10	20.3	-1.57	28.8	2.23	0.60	0.15	4.5	-1.38
DP-FETA	114.0	3.30	0.63	0.02	18.6	-2.22	137.0	1.81	0.68	0.03	14.6	-1.53	24.8	2.30	0.63	0.17	3.5	-1.26
PDP-Diffusion	19.9	8.28	0.53	0.64	9.1	-2.25	24.2	3.39	0.57	0.61	4.8	-1.62	8.1	2.73	0.53	0.61	2.2	-1.09
DP-LDM (SD)	19.8	8.39	0.53	0.63	8.94	-2.25	29.7	3.39	0.49	0.60	6.7	-1.68	24.1	3.15	0.38	0.64	5.1	-1.49
DP-LDM	51.5	6.08	0.57	0.39	12.4	-2.26	69.6	3.06	0.42	0.27	15.3	-1.96	40.4	3.02	0.40	0.40	6.7	-1.65
DP-LoRA	29.1	7.71	0.54	0.57	9.25	-2.26	50.9	3.23	0.46	0.36	12.8	-1.93	32.2	3.03	0.38	0.52	6.0	-1.62
PrivImage	21.4	8.08	0.54	0.62	8.9	-2.24	24.2	3.75	0.49	0.66	5.4	-1.69	11.3	2.88	0.50	0.61	2.9	-1.25

- **RQ3:** How does pretraining with public datasets affect the performance of synthetic images?
- **RQ4:** Can we combine various methods to further enhance synthetic performance?

We provide the computational resources and runtime analysis of studied methods in Table 19 of Appendix D.

7.1. The Quality of Synthetic Images (RQ1)

Experiment Design. To answer RQ1, this section first studies the utility and fidelity of synthetic images generated by the studied methods under privacy budgets of $\epsilon = \{1, 10\}$. We also provide visualizations to offer intuitive presentations. The synthesizer sizes for the GAN-based and diffusion-based methods are 5.4M and 3.8M. For GAN-based methods, we use BigGAN [82], which is a widely used GAN model, with a default generator size of 3.8M and a discriminator size of 1.6M. Thus, the generators used in GAN-based and diffusion-based methods are nearly identical. For diffusion-based methods, we follow the model size settings from DPDM [31] and PrivImage [4]. Besides, for latent diffusion-based methods such as DP-LDM and DP-LoRA, as described in Section 2.2, LDMs integrate an autoencoder into the diffusion process. The DMs remain consistent with other diffusion-based methods (the size of 3.8M), while the autoencoder follows the implementation provided in the original repositories of DP-LDM [18] and DP-LoRA [19]. We provide more descriptions of network architecture in Appendix B.2.2.

The high-dimensional sensitive datasets with resolutions larger than 32×32 are resized to 32×32 for fair comparison, following previous works [4], [31], [32]. We also tested higher image resolutions for CelebA, including 64×64 and 128×128 . It is noticed that without specific explanation, the following utility evaluations of this paper are obtained under the ‘Noisy SenV’ method.

Result Analysis. Tables 7 and 8 show the Acc of classifiers trained on the synthetic images. The best score of each column is marked with the gray color box. Table 9 reports the fidelity results under $\epsilon = 10$. Figure 4 illustrates the examples of synthetic images under $\epsilon = 10$. Notably, we leverage different experimental settings compared to the original papers, including changes to the model architecture, failure probability δ , and evaluation methods. These differences can lead to variations in performance relative to the results reported in the original publications. These results highlight the following key takeaways:

Directly tuning classifiers using the sensitive dataset overestimates the utility of synthetic images. For example, in Table 7, for the DP-Kernel method with the sensitive dataset EuroSAT, using the synthetic dataset as the validation set results in an accuracy decrease of 21.2% and 24.9% under $\epsilon = \{1, 10\}$. Tables 7 and 8 present the average results for Noisy SenV’ and SynV’, showing a decrease of 1.33% and 4.48% in accuracy under $\epsilon = 1$, and 1.12% and 3.00% under $\epsilon = 10$, compared to the ‘SenV’ evaluation method. As ϵ increases, the quality of synthetic images improves, leading to reduced utility evaluation errors. These results



Figure 4: The examples of synthetic images under $\epsilon = 10$ and $\delta = 1/N \log(N)$. The last row of images are real image samples from each sensitive image dataset.

also indicate that the ‘Noisy Senv’ method achieves better utility evaluation than the ‘SynV.’

Our fidelity and utility evaluation provides a more comprehensive view of the quality of synthetic images.

IS focuses on evaluating the practical quality of synthetic images. However, its ability to evaluate unnatural images, such as MNIST, FashionMNIST, and EuroSAT, remains limited [61]. In Table 9, the PE generates images with IS scores of 2.79, 5.37, 14.97, 19.65, 8.16, 3.87, and 4.58 for the seven sensitive datasets; six out of seven datasets achieve the highest IS across all methods. However, despite the high practical quality of these images, they are not of good utility, achieving Acc scores of 32.7%, 57.8%, 75.3%, 24.9%, 36.8%, 74.2%, and 64.9%. Five out of seven of them are lower than the best methods.

For DP-LDM and DP-LoRA for MNIST, the Acc under $\epsilon = 10$ is 95.5% and 97.1%, but the FID is 99.1 and 95.4. The synthetic images retain essential information for downstream models but may lack realistic textures, colors, and fine details, as these methods prioritize class-discriminative features like shapes over photorealism. In their original implementations, DP-LDM and DP-LoRA resize MNIST images to 32×32 , whereas the original size of MNIST image is 28×28 . This resizing results in better FID scores reported in their paper compared to DImageBench. When resizing to 32×32 , DP-LDM and DP-LoRA in DImageBench achieve FID scores of 13.4 and 12.1, similar to what was reported in their papers. Precision and Recall are decoupled from FID, meaning that having one value high and the other low does not necessarily improve the FID for synthetic images. For example, in the case of DPGAN with CIFAR-10, the precision is 0.67, the best among all methods. However, its recall is as low as 0.01, and the FID is as high as 138.7. FLD considers the novelty of synthetic images, and better FLD scores generally indicate that most other fidelity metrics are also favorable. The human perspective metric, IR, is consistently negative due to the resolution of synthetic images being 32×32 , which is lower than that of text-to-image synthetic images presented in paper [25], which are

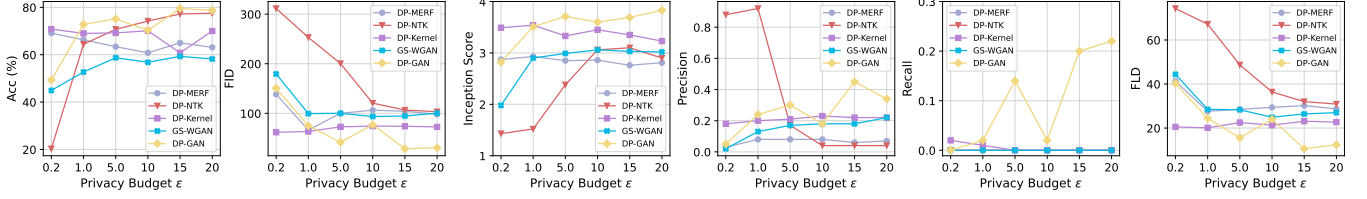
TABLE 10: The Acc and FID of synthetic images using CelebA as the sensitive dataset under $\epsilon = 10$, with varying synthetic image resolutions. The best and second-best results are highlighted in bold and underlined.

Algorithm (CelebA)	32×32		64×64		128×128	
	Acc	FID	Acc	FID	Acc	FID
DP-MERF	81.2	147.9	61.7	381.2	61.4	311.2
DP-NTK	64.2	346.6	64.2	299.9	62.9	272.1
DP-Kernel	83.7	128.8	73.5	272.4	53.7	359.2
PE	74.2	22.0	70.2	<u>26.8</u>	68.9	59.4
GS-WGAN	61.5	290.0	61.8	433.6	61.4	383.2
DP-GAN	89.2	31.7	61.8	395.0	39.9	320.2
DPDM	91.8	28.8	78.7	106.7	71.1	210.8
DP-FETA	94.2	24.8	82.6	89.4	69.3	173.6
PDP-Diffusion	<u>94.0</u>	8.1	92.7	91.7	74.1	121.1
DP-LDM (SD)	89.1	24.1	84.3	117.8	67.3	188.6
DP-LDM	92.4	40.4	90.2	110.7	83.6	156.1
DP-LoRA	92.0	32.2	82.6	99.2	78.0	169.9
PrivImage	92.0	11.3	91.3	23.6	61.2	106.3
Average	84.0	87.5	76.6	188.4	65.6	218.4

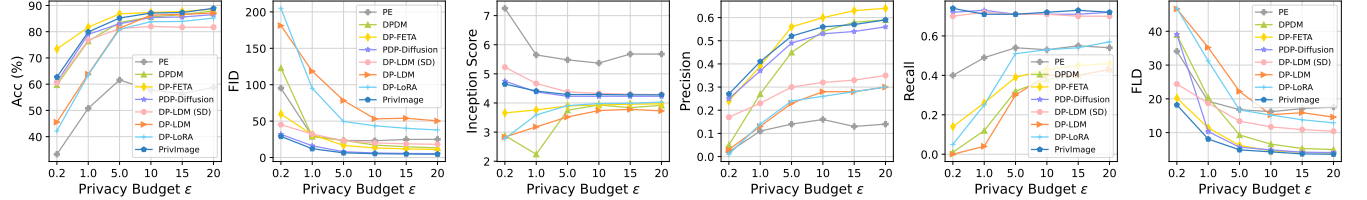
1024×1024 . We provide more details of fidelity evaluations for the Camelyon in Appendix D.

Current methods still face challenges in high-resolution DP image synthesis.

Table 10 shows the Acc and FID of synthetic CelebA with varying resolutions. As the resolution of synthetic images increases from 32×32 to 128×128 , the average accuracy and FID of synthetic images drop from 84.0 and 87.5 to 65.6 and 218.4, respectively. Current methods still struggle with synthesizing high-resolution images. However, PE is the least affected by the increased resolutions in synthetic images, as the synthetic images of PE only depend on the capability of foundational APIs. Other methods, such as PrivImage and DP-LDM, which train synthesizers using DP-SGD, fail in high-resolution image synthesis. High-resolution images contain more complex spatial structures, requiring more precise gradients to capture meaningful patterns. However, DP-SGD injects noise into gradients, which disrupts these updates. As image resolution increases, the number of model parameters and/or the number of required model updates also grows, making it harder for DP-SGD to converge. Note that we leverage the default

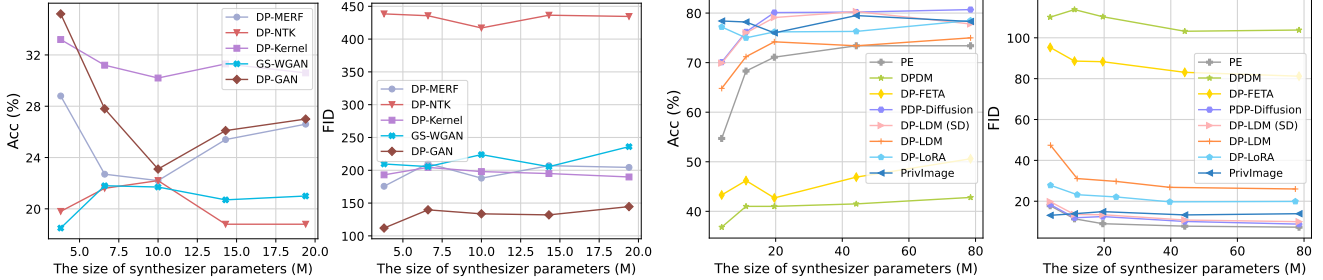


(a) Five GAN-Based investigated methods.



(b) Eight diffusion-based investigated methods.

Figure 5: The utility and fidelity of synthetic images generated by the studied methods for FashionMNIST dataset under privacy budgets $\epsilon = \{0.2, 1.0, 5.0, 10.0, 15.0, 20.0\}$ and a fixed $\delta = 1/N \log(N)$.



(a) GAN-Based Synthesizers.

(b) diffusion-based Synthesizers.

Figure 6: The Acc and FID of synthetic images generated by the studied algorithms for CIFAR-10 dataset under privacy budgets $\epsilon = 10$. For diffusion-based synthesizers, we consider sizes of $\{3.8M, 10.0M, 20.0M, 40.0M, 80.0M\}$, while for the model size of GAN-based synthesizers, we use $\{3.8M, 6.6M, 10.0M, 14.3M, 19.4M\}$.

parameter size of synthesizers, which is 3.8M. A larger size of synthesizers may improve the synthetic performance.

7.2. Model Architecture and Privacy Budget (RQ2)

Experiment Design. We study the utility and fidelity of synthetic images of studied methods across five distinct privacy budgets $\epsilon = \{0.2, 1.0, 5.0, 10.0, 20.0\}$. This RQ also studies how the DP image synthesis methods perform under different sizes of synthesizers. We further evaluate the performance of DP image synthesis methods with varying synthesizer sizes under a certain privacy budget $\epsilon = 10$. For diffusion-based synthesizers, we consider sizes of $\{3.8M, 10.0M, 20.0M, 40.0M, 80.0M\}$, while for the model size of GAN-based synthesizers, we use $\{3.8M, 6.6M, 10.0M, 14.3M, 19.4M\}$.

Result Analysis. Figure 5 presents the utility and fidelity evaluations of synthetic images on the FashionMNIST dataset under different privacy budgets. Figure 6 presents the evaluations of synthetic images for CIFAR-10 across

different model sizes. The results, presented in Fig 5 and Figure 6, highlight the following key takeaways:

Adding noise on low-dimensional features is less sensitive to privacy budgets. Figure 5 shows that adding noise to high-dimensional features, like weight gradients, generally yields superior synthesis performance compared to adding noise to low-dimensional features, such as adding noise to training loss in DP-Kernel, especially when the privacy budget is large (e.g., $\epsilon = 10$ and 20). However, methods that add noise to high-dimensional features are more sensitive to the privacy budget. At very low privacy budgets, such as $\epsilon = 0.2$, methods that add noise to low-dimensional features outperform, with DP-Kernel and DP-MERF achieving the highest accuracy of 71.2% and 70.6%. These low-dimensional features exhibit lower sensitivity, allowing for a smaller noise scale than the noise scale added to high-dimensional features.

Larger synthesizer models do not always yield better performance. GANs often encounter unstable training [39], [83] and mode collapse issues [84], [85]. Training a larger GAN model under DP is even more challenging. As a result,

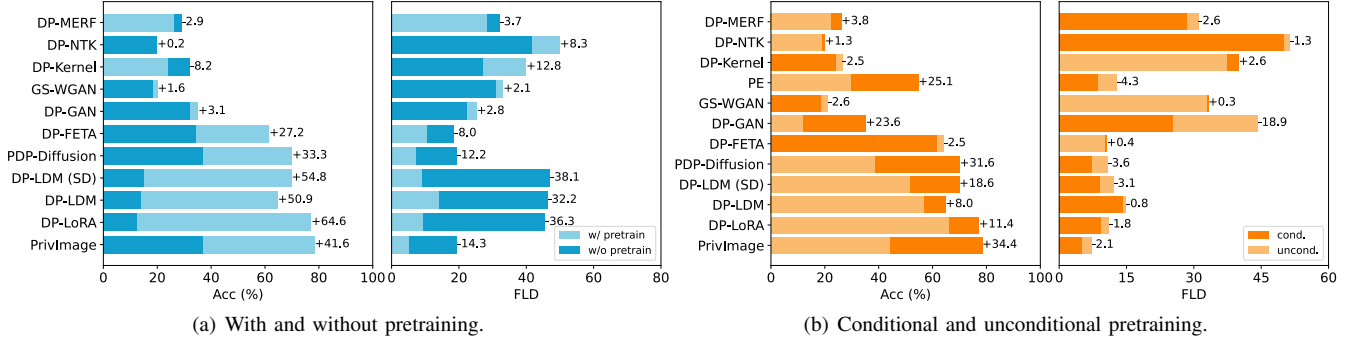


Figure 7: The Acc and FLD evaluations of synthetic images under $\epsilon = 10$ and $\delta = 1/N \log(N)$ for the CIFAR-10 dataset. The labels ‘w/ pretrain’ and ‘w/o pretrain’ refer to the studied algorithms with and without pretraining. ‘cond.’ and ‘uncond.’ indicate the use of conditional and unconditional pretraining. The relative changes indicate the result of ‘w/ pretrain’ minus that of ‘w/o pretrain’, and the result of ‘cond.’ minus that of ‘uncond.’.

TABLE 11: The Acc of synthetic images generated by PrivImage under $\epsilon = 10$, using the sensitive dataset CIFAR-10.

Batch size	$M = 3.8M$	$M = 11.1M$	$M = 19.6M$	$M = 44.2M$
4,096	78.4	78.2	76.0	79.5
16,384	78.5	78.6	78.8	79.5

as seen in Figure 6, scaling up model sizes does not necessarily benefit GAN-based methods. A similar phenomenon can be observed in diffusion-based methods. For instance, in PrivImage, the accuracy of synthetic images decreases from 78.2% to 76.0% as the synthesizer size grows from 11.1M to 19.6M. Although larger synthesizers can better learn to generate high-quality synthetic images, the noise added to the gradient increases with model size under the same privacy budget, which can potentially degrade synthetic performance. Li et al. [4] demonstrated that when a synthesizer reaches the upper limit of its generalization capability—where increasing the model’s parameter size no longer improves synthesis performance—DP can further degrade results, with larger synthesizers potentially performing worse. One solution is to increase the batch size of DP-SGD to reduce the DP noise scale [86]. Table 11 presents the Acc of synthetic images from PrivImage with batch sizes of 4,096 and 16,384 (the batch size used in PrivImage [4]). We observe that the large batch size of DP-SGD is better for large model sizes.

7.3. Leveraging Public Image Datasets (RQ3)

Experiment Design. This RQ examines how pretraining on public image datasets benefits DP image synthesis under a privacy budget $\epsilon = 10$ from three perspectives as follows.

- We compare the performance of DP image synthesizers with and without pretraining on a public dataset.
- We compare the synthesis performance between unconditional and conditional pretraining. Details of the pretraining methods are provided in Appendix B.2.3.
- We compare the performance of synthesizers with different pretraining datasets, ImageNet and Places365.

TABLE 12: The Acc and FLD of synthetic images generated by PDP-Diffusion and PrivImage under $\epsilon = 10$, using the sensitive dataset MNIST and public dataset ImageNet with different pretraining iterations.

PDP-Diffusion	25K	50K	100K	200K	400K
Acc (%)	97.4	97.6	97.4	97.4	97.1
FLD	2.48	2.56	2.83	3.40	3.00
PrivImage	25K	50K	100K	200K	400K
Acc (%)	97.8	97.4	97.5	97.8	97.2
FLD	2.23	2.48	2.62	2.80	2.90

The default pretraining strategy is introduced in Appendix B.2.3. As described in Section 4.1.2, GS-WGAN pretrains synthesizers using the sensitive dataset without the need for external public datasets, unlike other methods such as PrivImage [4], PDP-Diffusion [32], and DP-LDM [18]. PrivImage and PDP-Diffusion both build upon DPDM but use a distinct pretraining method. Without pretraining, they both revert to the original DPDM.

Result Analysis. The key takeaways from this section are as follows:

Pretraining is more beneficial for diffusion-based methods than for GAN-based methods. Figure 7 shows the Acc and FLD of synthetic images for CIFAR-10, comparing results with and without pretraining, and examining both conditional and unconditional pretraining methods. The bar on the left indicates lower values, while the bar on the right indicates higher values. This figure shows that for diffusion-based methods, pretraining consistently improves both the utility and fidelity of synthetic images, while its impact on GAN-based methods varies. For example, for DP-Kernel, the Acc shows an 8.2% reduction while pretraining the synthesizer. GAN-based models have limited ability to produce high-quality images, so pretraining has less effect on their performance than it does for diffusion-based methods.

Conditional pretraining significantly outperforms unconditional pretraining. For example, in Figure 7, using unconditional pretraining for PrivImage results in a 34.4%

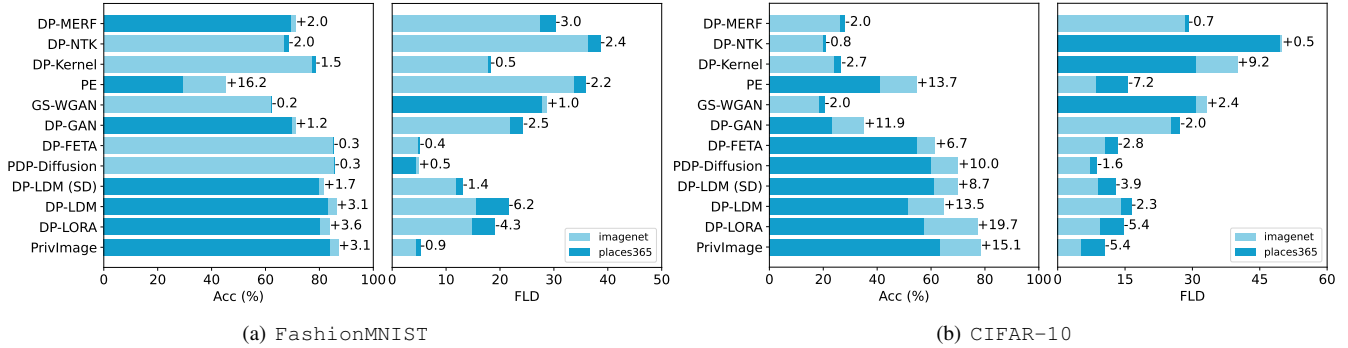


Figure 8: The Acc and FLD evaluations of synthetic images under $\epsilon = 10$ and $\delta = 1/N \log(N)$ for the sensitive datasets FashionMNIST and CIFAR-10, as well as the public datasets ImageNet and Places365. The relative changes represent the difference in performance between images pretrained on ImageNet and those pretrained on Places365.

TABLE 13: The Acc and FLD of synthetic CIFAR-10 images under $\epsilon = 10$, using the different subsets of ImageNet. ‘5%’ means matching categories from the sensitive CIFAR10 dataset in ImageNet (50 out of the 1000 available categories) using PrivImage. ‘5% rand.’ refers to 5% categories randomly selected. In each table, the first four methods above the horizontal line are GAN-based, while the remaining methods are diffusion-based.

Acc (%)	5%	5% (rand.)	5%+5% (rand.)	10% (rand.)	Whole
DP-MERF	22.1	25.1	18.1	23.7	26.1
DP-NTK	22.0	22.3	19.8	20.0	20.0
DP-Kernel	26.7	28.3	30.1	29.2	24.0
DP-GAN	24.9	18.6	21.0	21.1	28.1
PE	67.7	52.6	39.4	37.9	54.7
DP-FETA	62.2	49.2	65.0	51.5	61.4
PDP-Diffusion	78.9	53.8	73.7	59.5	70.1
DP-LDM (SD)	74.8	55.2	73.3	57.8	69.9
DP-LDM	68.3	55.2	62.9	58.2	64.8
DP-LoRA	78.2	70.5	75.9	69.7	77.2
FLD	5%	5% (rand.)	5%+5% (rand.)	10% (rand.)	Whole
DP-MERF	30.2	31.6	29.8	29.7	28.4
DP-NTK	50.0	50.5	55.9	53.6	49.8
DP-Kernel	31.5	30.1	30.3	31.1	30.0
DP-GAN	18.9	18.9	21.8	21.6	29.5
PE	4.5	6.5	12.2	10.6	8.5
DP-FETA	10.7	12.4	9.3	12.8	10.6
PDP-Diffusion	4.7	10.7	6.1	9.3	7.2
DP-LDM (SD)	5.1	11.7	7.2	10.6	9.0
DP-LDM	12.2	15.2	13.0	14.4	14.1
DP-LoRA	8.1	11.5	8.0	11.4	9.3

drop in accuracy and a 2.1 increase in FLD. The reason is that using labels for conditional pretraining helps establish a stronger connection between the labels and the images. On the other hand, when using the entire public dataset for pretraining, the presence of various labels unrelated to the sensitive images can cause the model to learn redundant label-to-image mappings. This distraction can compromise its ability to learn the meaningful and relevant features necessary for accurately synthesizing sensitive images. Table 12 also shows that excessive pretraining may reduce the performance of synthetic images.

A closer distribution match between the pretraining

distribution and the sensitive dataset improves DP image synthesis. PrivImage, which selects a subset of public images whose distribution closely matches that of the sensitive images, produces synthetic images with the highest utility on CIFAR-10 in Table 8. To further investigate the impact of the relationship between pretraining datasets and sensitive datasets on DP synthesis performance, Figure 8 compares the Acc and FLD for the sensitive datasets FashionMNIST and CIFAR-10 when pretraining with public datasets ImageNet and Places365. The average accuracy scores for CIFAR-10 using ImageNet and Places365 as the pretraining datasets are 48.3 and 42.3, respectively. For FashionMNIST, the average accuracy scores with ImageNet and Places365 are 77.2 and 76.1. Actually, ImageNet’s distribution is closer to CIFAR-10 than Places365 because its *object-focused* categories align more with CIFAR-10’s content [59]. Places365, focused on scenes [68], introduces less relevant background information, making its distribution less similar to CIFAR-10’s object-centric data. For GAN-based methods, pretraining offers minimal improvement, with performance varying slightly depending on whether ImageNet or Places365 is used. In contrast, for diffusion-based methods, pretraining enhances performance, as shown in Figure 7. Pretraining on ImageNet consistently outperforms Places365, except in the case of PDP-Diffusion trained on FashionMNIST, where the difference is marginal (0.3%).

7.4. Combining Algorithmic Improvement (RQ4)

Experiment Design. This RQ explores the potential of integrating the strengths of various methods to enhance existing approaches, laying the groundwork for future DP image synthesis methods.

- *Combining PrivImage with others.* We construct four subsets from the public dataset ImageNet and compare the synthesis performance when using different subsets for pretraining. These subsets are obtained by (1) randomly selecting 5% of images; (2) randomly selecting 10% of images; (3) using the distribution matching method in

PrivImage to select 5%, ensuring that the chosen subset matches the semantic distribution of the sensitive dataset; and (4) combining 5% from PrivImage with an additional 5% randomly selected. PrivImage is equivalent to PDP-Diffusion with 5% selected pretraining data.

- *Combining DP-FETA with others.* We incorporate a shortcut process into the DP training, extending it to other methods. Specifically, we extract central images from sensitive datasets and train synthesizers on these images prior to training on the sensitive images. Central images are perturbed with Gaussian noise for DP. PE is a fine-tuning-free method, so we exclude it from this analysis.

Privacy Analysis. Since both the data selection of PrivImage and central image constructions of DP-FETA will introduce additional privacy costs, combining them with other methods needs privacy composition. Considering the nice linearly composability property of Renyi DP (RDP) [34], we implement other methods with RDP, and use RDP to compose the privacy costs of two processes.

Result Analysis. Table 13 presents the results of using just 5% of a public dataset, aligned with the categories of CIFAR-10. Table 14 shows the results of integrating the DP training shortcut into other methods. These results highlight the following key takeaways:

Integrating the pretraining dataset selection proposed in PrivImage can enhance synthetic performance. The pretraining dataset selection improves the similarity between the public dataset and the sensitive dataset, and leads to accuracy improvements of 8.8% ($= 78.9\% - 70.1\%$) for PDP-Diffusion and 4.9% ($= 74.8\% - 69.9\%$) for DP-LDM (SD), respectively. For diffusion-based methods, the FLD of synthetic images is consistently better when pretraining synthesizers with 5% of a public dataset compared to using the entire dataset. Compared to randomly selecting images from the public dataset, there are performance decreases in Acc and FID when using the entire public dataset for pretraining. The improvement for GAN-based methods is minimal because GANs struggle more than DMs to learn the distribution of the public dataset. These results indicate that the relationship between the distributions of public and sensitive datasets plays a crucial role in improving synthetic image performance, which aligns with findings in other data domains [13]. This experiments also present efforts that incorporate the strength of selecting public datasets as proposed taxonomy in Section 4 to enhance methods.

Building DP training shortcut may damage the synthetic performance. Table 14 shows that incorporating a DP training shortcut may impair the synthetic performance of methods with pretraining. For instance, the Acc and FLD of DP-LDM (SD) decline from 81.6% and 11.7 to 80.6% and 13.3 when shortcuts are added. This is because the shortcut includes training on the central images after pretraining, which may damage the pretraining synthesizer. For methods without pretraining, the fidelity of synthetic images (measured by FLD) is consistently improved, while the improvement of utility (measured by Acc) fluctuates.

We hypothesize that the DP shortcut may disrupt the pretraining process, whereas pretraining dataset selection

TABLE 14: The Acc and FLD of synthetic images using FashionMNIST ($\epsilon = 10$). These methods integrate shortcuts for DP training proposed in DP-FETA.

Algorithm (CIFAR-10)	With DP Training Shortcuts		Original	
	Acc \uparrow (%)	FLD \downarrow	Acc \uparrow (%)	FLD \downarrow
DP-MERF	57.7	24.5	62.2	29.2
DP-NTK	70.6	31.0	76.3	36.4
DP-Kernel	78.0	18.5	70.0	21.3
GS-WGAN	58.9	27.2	56.7	28.1
DP-GAN	55.4	22.8	70.3	23.9
DPDM	87.3	4.6	85.6	6.6
PDP-Diffusion	85.0	4.7	85.4	4.9
DP-LDM (SD)	80.6	13.3	81.6	11.7
DP-LDM	85.3	18.8	86.3	15.4
DP-LoRA	86.3	14.2	83.8	14.8
PrivImage	86.4	4.6	87.1	4.3
Average	75.6	16.7	76.8	17.9

does not affect other algorithmic components. We need further research to effectively integrate the strengths of diverse algorithms.

8. Related Work

Several studies have established benchmarks for studying the role of DP in preserving the privacy of machine learning models [1], [3], [21], [22], [87]. However, Du et al. [3] and Tao et al. [87] focus exclusively on DP tabular data synthesis. Hu et al. [1] publish a systematization of knowledge on DP dataset synthesis covering various types of data, including tabular and graph data, among others. However, they overlook DP image synthesizers involving pretraining [4], [24] and foundational APIs [5]. Ganey et al. [22] propose a benchmark tailored for PATE-GAN. DPImageBench is the first benchmark to incorporate state-of-the-art synthesizers, such as DMs, and pretraining techniques for the DP image synthesis field.

9. Conclusions

DP image synthesis faces challenges due to complex codebases, inconsistent hyper-parameters, diverse model architectures, and the absence of standardized evaluation metrics. Advancing DP image synthesis algorithms requires a thorough understanding of existing methods and fair, direct comparisons. This paper introduces DPImageBench, a benchmark for evaluating DP image synthesis algorithms. First, in terms of *methods*, we analyze and systematically characterize twelve prominent approaches, detailing their model architectures, pretraining strategies, and privacy mechanisms. Our novel taxonomy examines where the noise is added to satisfy DP, enabling the exploration of combined DP image synthesis methods. Second, for *evaluation*, we use seven private datasets, two public datasets, and seven fidelity and utility metrics. Our findings reveal that selecting downstream classifiers based on the highest accuracy on the sensitive test set violates DP and inflates utility scores. DPImageBench addresses and corrects these issues. Third, the *platform* offers a standardized interface, enabling unified implementation for current and future methods.

Our analysis yields several key insights. Notably, we highlight that pretraining on public image datasets does not universally improve performance. Instead, the distributional similarity between pretraining and sensitive images plays a crucial role and can sometimes limit the benefits. Besides, we find that current methods still face challenges in high-resolution DP image synthesis. These findings highlight potential research opportunities for optimizing pretraining strategies to enhance DP image synthesis.

References

- [1] Y. Hu, F. Wu, Q. Li, Y. Long, G. Garrido, C. Ge, B. Ding, D. Forsyth, B. Li, and D. Song, "Sok: Privacy-preserving data synthesis," in *IEEE Symposium on Security and Privacy (SP)*, pp. 2–2, 2024.
- [2] Z. Lin, *Data Sharing with Generative Adversarial Networks: From Theory to Practice*. PhD thesis, Carnegie Mellon University, 2022.
- [3] Y. Du and N. Li, "Towards principled assessment of tabular data synthesis algorithms," *arXiv preprint arXiv:2402.06806*, 2024.
- [4] K. Li, C. Gong, Z. Li, *et al.*, "PrivImage: Differentially private synthetic image generation using diffusion models with Semantic-Aware pretraining," in *33rd USENIX Security Symposium (USENIX Security 24)*, pp. 4837–4854, 2024.
- [5] Z. Lin, S. Gopi, J. Kulkarni, H. Nori, and S. Yekhanin, "Differentially private synthetic data via foundation model APIs 1: Images," in *The Twelfth International Conference on Learning Representations*, 2024.
- [6] Z. Lin, T. Baltrusaitis, and S. Yekhanin, "Differentially private synthetic data via apis 3: Using simulators instead of foundation model," *arXiv preprint arXiv:2502.05505*, 2025.
- [7] K. Cai, X. Lei, J. Wei, and X. Xiao, "Data synthesis via differentially private markov random fields," *Proc. VLDB Endow.*, vol. 14, p. 2190–2202, July 2021.
- [8] R. McKenna, B. Mullins, D. Sheldon, and G. Miklau, "AIM: an adaptive and iterative mechanism for differentially private synthetic data," *Proc. VLDB Endow.*, vol. 15, no. 11, pp. 2599–2612, 2022.
- [9] X. Yue, H. Inan, X. Li, *et al.*, "Synthetic text generation with differential privacy: A simple and practical recipe," in *Proceedings of the 61st Annual Meeting of the Association for Computational Linguistics*, pp. 1321–1342, July 2023.
- [10] C. Xie, Z. Lin, A. Backurs, *et al.*, "Differentially private synthetic data via foundation model apis 2: Text," in *Forty-first International Conference on Machine Learning*, 2024.
- [11] D. Yu, S. Gopi, J. Kulkarni, Z. Lin, S. Naik, T. L. Religa, J. Yin, and H. Zhang, "Selective pre-training for private fine-tuning," *arXiv preprint arXiv:2305.13865*, 2023.
- [12] Z. Lin, A. Jain, C. Wang, G. Fanti, and V. Sekar, "Using gans for sharing networked time series data: Challenges, initial promise, and open questions," in *Proceedings of the ACM internet measurement conference*, pp. 464–483, 2020.
- [13] Y. Yin, Z. Lin, M. Jin, G. Fanti, and V. Sekar, "Practical gan-based synthetic ip header trace generation using netshare," in *Proceedings of the ACM SIGCOMM 2022 Conference*, pp. 458–472, 2022.
- [14] D. Sun, J. Q. Chen, C. Gong, T. Wang, and Z. Li, "Netdpsyn: synthesizing network traces under differential privacy," in *Proceedings of the 2024 ACM on Internet Measurement Conference*, pp. 545–554, 2024.
- [15] D. Chen, T. Orekondy, and M. Fritz, "GS-WGAN: A gradient-sanitized approach for learning differentially private generators," in *Advances in Neural Information Processing Systems*, 2020.
- [16] J. Jordon, J. Yoon, and M. van der Schaar, "PATE-GAN: generating synthetic data with differential privacy guarantees," in *7th International Conference on Learning Representations, ICLR*, 2019.
- [17] D. Jiang, S. Sun, and Y. Yu, "Functional renyi differential privacy for generative modeling," in *Advances in Neural Information Processing Systems*, 2023.
- [18] M. F. Liu, S. Lyu, M. Vinaroz, and M. Park, "Differentially private latent diffusion models," *arXiv preprint arXiv:2305.15759*, 2023.
- [19] Y.-L. Tsai, Y. Li, Z. Chen, P.-Y. Chen, C.-M. Yu, X. Ren, and F. Buet-Golfouse, "Differentially private fine-tuning of diffusion models," *arXiv preprint arXiv:2406.01355*, 2024.
- [20] D. Chen, R. Kerkouche, and M. Fritz, "A unified view of differentially private deep generative modeling," *arXiv:2309.15696*, 2023.
- [21] C. Wei, M. Zhao, Z. Zhang, *et al.*, "Dpmlbench: Holistic evaluation of differentially private machine learning," in *Proceedings of the 2023 ACM SIGSAC Conference on Computer and Communications Security*, pp. 2621–2635, 2023.
- [22] G. Ganev, M. S. M. S. Annamalai, and E. De Cristofaro, "The elusive pursuit of replicating pate-gan: Benchmarking, auditing, debugging," *arXiv preprint arXiv:2406.13985*, 2024.
- [23] M. Heusel, H. Ramsauer, T. Unterthiner, *et al.*, "Gans trained by a two time-scale update rule converge to a local nash equilibrium," *Advances in neural information processing systems*, vol. 30, 2017.
- [24] H. Wang, S. Pang, Z. Lu, *et al.*, "dp-promise: Differentially private diffusion probabilistic models for image synthesis," in *33rd USENIX Security Symposium*, pp. 1063–1080, 2024.
- [25] J. Xu, X. Liu, Y. Wu, *et al.*, "Imagereward: Learning and evaluating human preferences for text-to-image generation," *Advances in Neural Information Processing Systems*, vol. 36, 2024.
- [26] K. Li, C. Gong, X. Li, Y. Zhao, X. Hou, and T. Wang, "From easy to hard: Building a shortcut for differentially private image synthesis," *arXiv preprint arXiv:2504.01395*, 2025.
- [27] T. Salimans, I. Goodfellow, W. Zaremba, V. Cheung, A. Radford, and X. Chen, "Improved techniques for training gans," *Advances in neural information processing systems*, vol. 29, 2016.
- [28] F. Harder, K. Adamczewski, and M. Park, "DP-MERF: differentially private mean embeddings with random features for practical privacy-preserving data generation," in *AISTATS*, pp. 1819–1827, 2021.
- [29] Y. Yang, K. Adamczewski, and *et al.*, "Differentially private neural tangent kernels for privacy-preserving data generation," *CoRR*, vol. abs/2303.01687, 2023.
- [30] L. Xie, K. Lin, and *et al.*, "Differentially private generative adversarial network," *CoRR*, vol. abs/1802.06739, 2018.
- [31] T. Dockhorn, T. Cao, A. Vahdat, *et al.*, "Differentially private diffusion models," *Transactions on Machine Learning Research*, 2023.
- [32] S. Ghalebikesabi, L. Berrada, S. Gowal, *et al.*, "Differentially private diffusion models generate useful synthetic images," *CoRR*, vol. abs/2302.13861, 2023.
- [33] C. Dwork, F. McSherry, K. Nissim, and A. Smith, "Calibrating noise to sensitivity in private data analysis," in *Theory of Cryptography: Third Theory of Cryptography Conference*, pp. 265–284, 2006.
- [34] I. Mironov, "Renyi differential privacy," *CoRR*, vol. abs/1702.07476, 2017.
- [35] M. Abadi, A. Chu, I. J. Goodfellow, and *et al.*, "Deep learning with differential privacy," in *Proceedings of the ACM SIGSAC Conference on Computer and Communications Security*, pp. 308–318, 2016.
- [36] I. Mironov, K. Talwar, and L. Zhang, "Rényi differential privacy of the sampled gaussian mechanism," *CoRR*, vol. abs/1908.10530, 2019.
- [37] J. Ho, A. Jain, and P. Abbeel, "Denoising diffusion probabilistic models," in *Advances in Neural Information Processing Systems*, 2020.
- [38] R. Rombach, A. Blattmann, D. Lorenz, P. Esser, and B. Ommer, "High-resolution image synthesis with latent diffusion models," in *Proceedings of the IEEE/CVF conference on computer vision and pattern recognition*, pp. 10684–10695, 2022.

- [39] M. Arjovsky, S. Chintala, and L. Bottou, "Wasserstein generative adversarial networks," in *International conference on machine learning*, pp. 214–223, PMLR, 2017.
- [40] I. J. Goodfellow, J. Pouget-Abadie, M. Mirza, and et al., "Generative adversarial nets," in *Advances in Neural Information Processing Systems*, pp. 2672–2680, 2014.
- [41] A. Ramesh, P. Dhariwal, A. Nichol, et al., "Hierarchical text-conditional image generation with clip latents," *arXiv preprint arXiv:2204.06125*, p. 3, 2022.
- [42] P. Bándi, O. Geessink, Q. Manson, and et al., "From detection of individual metastases to classification of lymph node status at the patient level: The CAMELYON17 challenge," *IEEE Trans. Medical Imaging*, vol. 38, no. 2, pp. 550–560, 2019.
- [43] Z. Liu, P. Luo, X. Wang, and et al., "Deep learning face attributes in the wild," in *2015 IEEE International Conference on Computer Vision, ICCV 2015*, pp. 3730–3738, 2015.
- [44] T. Matsumoto, T. Miura, and N. Yanai, "Membership inference attacks against diffusion models," in *IEEE Security and Privacy Workshops (SPW)*, pp. 77–83, 2023.
- [45] A. Rahimi and B. Recht, "Random features for large-scale kernel machines," *Advances in neural information processing systems*, 2007.
- [46] A. Smola, A. Gretton, L. Song, and B. Schölkopf, "A hilbert space embedding for distributions," in *International conference on algorithmic learning theory*, pp. 13–31, Springer, 2007.
- [47] N. Aronszajn, "Theory of reproducing kernels," *Transactions of the American mathematical society*, vol. 68, no. 3, pp. 337–404, 1950.
- [48] A. Gretton, K. M. Borgwardt, M. J. Rasch, et al., "A kernel two-sample test," *J. Mach. Learn. Res.*, vol. 13, pp. 723–773, 2012.
- [49] F. Harder, M. Jalali, D. J. Sutherland, and et al., "Pre-trained perceptual features improve differentially private image generation," *Trans. Mach. Learn. Res.*, vol. 2023, 2023.
- [50] S. Arora, S. S. Du, W. Hu, et al., "On exact computation with an infinitely wide neural net," *Advances in neural information processing systems*, vol. 32, 2019.
- [51] A. Srivastava, L. Valkov, C. Russell, et al., "Veegan: Reducing mode collapse in gans using implicit variational learning," *Advances in neural information processing systems*, vol. 30, 2017.
- [52] C. Dwork, A. Roth, et al., "The algorithmic foundations of differential privacy," *Foundations and Trends® in Theoretical Computer Science*, vol. 9, no. 3–4, pp. 211–407, 2014.
- [53] T. Karras, M. Aittala, T. Aila, and S. Laine, "Elucidating the design space of diffusion-based generative models," in *Advances in Neural Information Processing Systems*, 2022.
- [54] A. Vaswani, "Attention is all you need," *Advances in Neural Information Processing Systems*, 2017.
- [55] E. J. Hu, Y. Shen, P. Wallis, et al., "Lora: Low-rank adaptation of large language models," in *The Tenth International Conference on Learning Representations, ICLR*, 2022.
- [56] J. Long and H. Lu, "Multi-level gate feature aggregation with spatially adaptive batch-instance normalization for semantic image synthesis," in *27th International Conference, MMM*, pp. 378–390, 2021.
- [57] O. Vinyals, A. Toshev, S. Bengio, and et al., "Show and tell: A neural image caption generator," in *IEEE Conference on Computer Vision and Pattern Recognition*, pp. 3156–3164, 2015.
- [58] K. Xu, J. Ba, R. Kiros, and et al., "Show, attend and tell: Neural image caption generation with visual attention," in *Proceedings of the 32nd International Conference on Machine Learning*, vol. 37, pp. 2048–2057, 2015.
- [59] J. Deng, W. Dong, R. Socher, and et al., "Imagenet: A large-scale hierarchical image database," in *IEEE Computer Society Conference on Computer Vision and Pattern Recognition CVPR*, 2009.
- [60] Z. Lin, V. Sekar, and G. Fanti, "On the privacy properties of gan-generated samples," in *International Conference on Artificial Intelligence and Statistics*, pp. 1522–1530, PMLR, 2021.
- [61] M. Jiralerspong, J. Bose, I. Gemp, et al., "Feature likelihood divergence: evaluating the generalization of generative models using samples," in *Thirty-seventh Conference on Neural Information Processing Systems*, 2023.
- [62] T. Kynkäänniemi, T. Karras, S. Laine, J. Lehtinen, and T. Aila, "Improved precision and recall metric for assessing generative models," *Advances in neural information processing systems*, vol. 32, 2019.
- [63] C. Szegedy, V. Vanhoucke, S. Ioffe, et al., "Rethinking the inception architecture for computer vision," in *Proceedings of the conference on computer vision and pattern recognition*, pp. 2818–2826, 2016.
- [64] Y. LeCun, L. Bottou, Y. Bengio, and et al., "Gradient-based learning applied to document recognition," *Proc. IEEE*, vol. 86, no. 11, pp. 2278–2324, 1998.
- [65] H. Xiao, K. Rasul, and R. Vollgraf, "Fashion-mnist: a novel image dataset for benchmarking machine learning algorithms," *CoRR*, 2017.
- [66] A. Krizhevsky, "Learning multiple layers of features from tiny images," tech. rep., University of Toronto, 2009.
- [67] P. Helber, B. Bischke, A. Dengel, and D. Borth, "Eurosat: A novel dataset and deep learning benchmark for land use and land cover classification," *IEEE Journal of Selected Topics in Applied Earth Observations and Remote Sensing*, vol. 12, pp. 2217–2226, 2019.
- [68] B. Zhou, A. Lapedriza, A. Khosla, et al., "Places: A 10 million image database for scene recognition," *IEEE transactions on pattern analysis and machine intelligence*, vol. 40, pp. 1452–1464, 2017.
- [69] N. Ponomareva, H. Hazimeh, A. Kurakin, et al., "How to dp-fy ml: A practical guide to machine learning with differential privacy," *Journal of Artificial Intelligence Research*, vol. 77, pp. 1113–1201, 2023.
- [70] X. Tang, R. Shin, H. A. Inan, A. Manoel, F. Mireshghallah, Z. Lin, S. Gopi, J. Kulkarni, and R. Sim, "Privacy-preserving in-context learning with differentially private few-shot generation," in *The Twelfth International Conference on Learning Representations*.
- [71] F. McSherry, "Privacy integrated queries: an extensible platform for privacy-preserving data analysis," in *Proceedings of the ACM International Conference on Management of Data*, pp. 19–30, 2009.
- [72] M. Nasr, S. Songi, A. Thakurta, et al., "Adversary instantiation: Lower bounds for differentially private machine learning," in *2021 IEEE Symposium on security and privacy (SP)*, pp. 866–882, IEEE, 2021.
- [73] M. S. M. S. Annamalai and E. De Cristofaro, "Nearly tight black-box auditing of differentially private machine learning," in *The Thirtieth Conference on Neural Information Processing Systems*, 2024.
- [74] M. S. M. S. Annamalai, G. Ganev, and E. D. Cristofaro, "what do you want from theory alone?" experimenting with tight auditing of differentially private synthetic data generation," in *33rd USENIX Security Symposium*, pp. 4855–4871, 2024.
- [75] T. Steinke, M. Nasr, and M. Jagielski, "Privacy auditing with one (1) training run," *Advances in Neural Information Processing Systems*, vol. 36, pp. 49268–49280, 2023.
- [76] M. Jagielski, J. Ullman, and A. Oprea, "Auditing differentially private machine learning: How private is private sgd?," *Advances in Neural Information Processing Systems*, vol. 33, pp. 22205–22216, 2020.
- [77] C. Schuhmann, R. Beaumont, R. Vencu, et al., "Laion-5b: An open large-scale dataset for training next generation image-text models," *Advances in Neural Information Processing Systems*, vol. 35, pp. 25278–25294, 2022.
- [78] 51CTO, "Privacy issues analysis of the laion-5b dataset." https://www.51cto.com/article/777427.html?utm_source=chatgpt.com, Mar. 2022.
- [79] S. Zagoruyko, "Wide residual networks," *arXiv preprint arXiv:1605.07146*, 2016.

- [80] S. Xie, R. Girshick, P. Dollár, *et al.*, “Aggregated residual transformations for deep neural networks,” in *IEEE Conference on Computer Vision and Pattern Recognition (CVPR)*, pp. 5987–5995, 2017.
- [81] K. He, X. Zhang, S. Ren, and J. Sun, “Deep residual learning for image recognition,” in *2016 IEEE Conference on Computer Vision and Pattern Recognition, CVPR*, pp. 770–778, 2016.
- [82] A. Brock, J. Donahue, and K. Simonyan, “Large scale GAN training for high fidelity natural image synthesis,” in *7th International Conference on Learning Representations, ICLR*, 2019.
- [83] Z. Lin, V. Sekar, and G. Fanti, “Why spectral normalization stabilizes gans: Analysis and improvements,” *Advances in neural information processing systems*, vol. 34, pp. 9625–9638, 2021.
- [84] Z. Lin, A. Khetan, G. Fanti, and S. Oh, “Pacgan: The power of two samples in generative adversarial networks,” *Advances in neural information processing systems*, vol. 31, 2018.
- [85] I. Goodfellow, “Nips 2016 tutorial: Generative adversarial networks,” *arXiv preprint arXiv:1701.00160*, 2016.
- [86] S. De, L. Berrada, J. Hayes, S. L. Smith, and B. Balle, “Unlocking high-accuracy differentially private image classification through scale,” *arXiv preprint arXiv:2204.13650*, 2022.
- [87] Y. Tao, R. McKenna, M. Hay, *et al.*, “Benchmarking differentially private synthetic data generation algorithms,” *arXiv:2112.09238*, 2021.

Appendix

Appendix A. Privacy Notations

As shown in Table 1, different definitions of neighboring datasets (i.e., replace-one, add-or-remove-one) have been used in prior work. In this section, we show that the methods that used the replace-one definition—DP-MERF, DP-NTK, and DP-Kernel—can all be adapted to the add-or-remove-one definition without affecting their (ϵ, δ) DP parameters.

Our key idea is to show that the *sensitivity* of the function these methods privatize remains the same when switching from replace-one to add-or-remove-one. For all these three methods, the function to be privatized is the *mean (vector or kernel) feature embedding of the private dataset*. For simplicity, we will use DP-MERF as an example, and the proof for the other two methods is similar. Let m be the number of private samples, and $\hat{\phi}(x)$ be the feature of sample x . Let the two neighboring datasets (under the replace-one definition) be $\mathcal{D} = \{x_1, \dots, x_m\}$ and $\mathcal{D}' = \{x'_1, \dots, x'_m\}$ where they only differ on the i -th sample: $x_i \neq x'_i$. Eq. (9) and (10) in DP-MERF [28] show that the sensitivity of the mean feature embedding is $\frac{2}{m}$:

$$\max_{\mathcal{D}, \mathcal{D}'} \left\| \frac{1}{m} \sum_{i=1}^m \hat{\phi}(x_i) - \frac{1}{m} \sum_{i=1}^m \hat{\phi}(x'_i) \right\| \leq \frac{2}{m}.$$

After we switch the definition to add-or-remove-one, without loss of generality, let us assume that $\mathcal{D} = \{x_1, \dots, x_{m-1}\}$

TABLE 15: Learning rate and batch size for training models.

Method	Learning Rate	Batch Size
DP-MERF	1×10^{-2}	100
DP-NTK	1×10^{-2}	4,096
DP-Kernel	3×10^{-4}	60
PE	-	-
GS-WGAN	1×10^{-4}	32
DP-GAN	3×10^{-4}	4,096
DPDM	3×10^{-4}	4,096
DP-FETA	3×10^{-4}	4,096
PDP-Diffusion	3×10^{-4}	4,096
DP-LDM (SD)	3×10^{-4}	4,096
DP-LDM	2×10^{-3}	4,096
DP-LoRA	2×10^{-3}	4,096
PrivImage	3×10^{-4}	4,096

and $\mathcal{D}' = \{x'_1, \dots, x'_m\}$, where $x_i = x'_i, i \in [1, \dots, m-1]$. In this case, the sensitivity is:

$$\begin{aligned} & \max_{\mathcal{D}, \mathcal{D}'} \left\| \frac{1}{m-1} \sum_{i=1}^{m-1} \hat{\phi}(x_i) - \frac{1}{m} \sum_{i=1}^m \hat{\phi}(x'_i) \right\| \\ &= \max_{\mathcal{D}, \mathcal{D}'} \left\| \frac{1}{m(m-1)} \sum_{i=1}^{m-1} \hat{\phi}(x_i) - \frac{1}{m} \hat{\phi}(x_m) \right\| \\ &\leq \frac{m-1}{m(m-1)} + \frac{1}{m} = \frac{2}{m}. \end{aligned}$$

In addition, this bound is tight. For example, when $\hat{\phi}(x_1) = \dots = \hat{\phi}(x_{m-1}) = 1$ and $\hat{\phi}(x_m) = -1$, the upper bound is achieved.

Appendix B. DP Image Synthesizer Details

B.1. Implementations

In all experiments, we used default hyper-parameter settings and made minimal modifications to public implementations whenever possible. PE utilizes discrete-step diffusion models, whereas DPDM, PDP-Diffusion, and PrivImage use continuous-step diffusion models. Discrete-step diffusion models proceed with fixed discrete time increments, whereas continuous-step diffusion models model diffusion as a continuous-time process using differential equations. We list the code bases of the investigated methods below.

- DP-MERF: <https://github.com/ParkLabML/DP-MERF>
- DP-Kernel: <https://github.com/dihjiang/DP-kernel>
- DP-NTK: <https://github.com/Justinyangjy/DP-NTK>
- PE: <https://github.com/microsoft/DPSDA>
- GS-WGAN: <https://github.com/DingfanChen/GS-WGAN>
- DP-GAN: <https://github.com/illidanlab/dpgan>
- DPDM: <https://github.com/nv-tlabs/DPDM>
- DP-FETA: <https://github.com/SunnierLee/DP-Pretrain>
- DP-LDM: <https://github.com/SaiyueLyu/DP-LDM>
- DP-LoRA: <https://github.com/EzzzLi/DP-LORA>
- PrivImage: <https://github.com/SunnierLee/DP-ImaGen>

Noted that PDP-Diffusion did not release their source code. Instead, we refer to the implementation provided by

TABLE 16: The number of iterations for training models.

Method	MNIST & F-MNIST	CIFAR-10 & CIFAR-100	EuroSAT	CelebA	Camelyon
DP-MERF	3,000	2,500	1,150	8,138	15,122
DP-NTK	2,000	2,000	2,000	2,000	2,000
DP-Kernel	200,002	200,002	200,002	200,002	200,002
PE	8	8	8	8	8
GS-WGAN	2,000	2,000	2,000	2,000	2,000
DP-GAN	2,196	1,830	842	3,974	3,692
DPDM	2,196	1,830	842	3,974	3,692
DP-FETA	2,196	1,830	842	3,974	3,692
PDP-Diffusion	2,196	1,830	842	3,974	3,692
DP-LDM (SD)	2,196	1,830	842	3,974	3,692
DP-LDM	2,196	1,830	842	3,974	3,692
DP-LoRA	2,196	1,830	842	3,974	3,692
PrivImage	2,196	1,830	842	3,974	3,692

the PrivImage repository, which uses PDP-Diffusion as a baseline. Additionally, the original DP-LDM repository implements a LDM. For a fair comparison, we use a standard diffusion model as the synthesizer to implement DP-LDM (SD), built upon the DPDM repository.

B.2. Hyper-parameter Settings

B.2.1. Investigated Synthesis Algorithms. This section elaborates on the hyper-parameter settings for DP image synthesis methods. Table 15 presents the learning rate and batch size, which are all the same on different datasets for each method. Table 16 presents the number of iterations for finetuning on sensitive datasets. We can calculate the number of iterations as $(\text{epoch} \times \text{size of sensitive data}) / (\text{batch size})$.

DP-MERF. The dimension of random Fourier features is 10,000, and the sigma for these features is 105.

DP-NTK. For the NTK model, We use fully-connected 1-hidden-layer and 2-hidden-layer neural network with the width $\{800\}$ and $\{32, 256\}$ for RGB and gray scale images.

DP-Kernel. The sigma used to calculated the kernel is set as $\{1, 2, 4, 8, 16\}$.

PE. Refer to the practical adoption in the original paper [5], we use the pretrained model “imagenet64_cond_270M_250K.pt” as the foundational API³. For generating 128×128 images, we use the pretrained model “128x128_diffusion.pt” as the foundational API⁴. These APIs are only trained on ImageNet.

GS-WGAN. We use 1,000 discriminators and 1 generator. The clip bound of the gradient is set as 2.0.

DP-GAN. We use BigGAN [82] as the synthesizer in our implementation of DP-GAN, resulting in improved synthesis performance compared to the original DP-GAN [30].

DPDM. We use continuous-time DMs following their code. We use the noise multiplicity proposed in their paper, and the multiplicity number is set as 32 for all datasets.

DP-FETA. We first pretrain diffusion models on the central images and then fine-tune the models on the sensitive dataset like DPDM. We query 10 central images for EuroSAT, 50 central images for MNIST, F-MNIST, and CIFAR-10, and 500 central images for CelebA and Camelyon.

3. <https://github.com/openai/improved-diffusion>

4. <https://github.com/openai/guided-diffusion>

TABLE 17: The hyper-parameters for pretraining DP image synthesizers on ImageNet. Since PrivImage only uses 5% public images for pretraining, we multiply its epoch by 20 to achieve the same training iterations as PDP-Diffusion.

Method	Iterations	Epoch	Learning Rate	Batch Size
DP-MERF	12,811	1	1×10^{-2}	100
DP-NTK	4,000	16	1×10^{-2}	5,000
DP-Kernel	20,018	1	5×10^{-5}	64
PE	-	-	-	-
GS-WGAN	40,036	1	1×10^{-4}	32
DP-GAN	200,182	160	3×10^{-4}	1,024
DPDM	200,182	160	3×10^{-4}	1,024
DP-FETA	2,000	2,000	3×10^{-4}	50
PDP-Diffusion	200,182	160	3×10^{-4}	1,024
DP-LDM (SD)	200,182	160	3×10^{-4}	1,024
DP-LDM	200,182	160	2×10^{-3}	1,024
DP-LoRA	200,182	160	2×10^{-3}	1,024
PrivImage	200,182	3,200	3×10^{-4}	1,024

PDP-Diffusion. We first pretrain diffusion models on the public dataset, and then fine-tune the models on the sensitive dataset like DPDM.

DP-LDM (SD). The pretraining stage is the same as PDP-Diffusion. During the finetuning, we only set the label embedding layer and attention modules trainable instead of all the modules in the diffusion model.

DP-LDM. During pretraining, we first pretrain a Variational AutoEncoder (VAE) on ImageNet, and then pretrain DM on the latent space of VAE. The finetuning stage is the same as DP-LDM (SD).

DP-LoRA. The pretraining stage is the same as DP-LDM. During finetuning, we use the LoRA [55] technique to finetune the label embedding layer and attention modules of DM.

PrivImage. We implement the semantic query function with ResNet-50, and its training epoch is set as 500. We select 5% public data for all sensitive datasets.

B.2.2. Network Architecture. For a fair comparison, we implement the GAN-based methods using the same network architecture of BigGAN generator [82] except for GS-WGAN for its poor performance. Specifically, the generator has a noise vector dimension of 60, a shared feature dimension of 128, and a convolutional feature dimension of 60. For DPDM, PDP-Diffusion, DP-LDM (SD), and PrivImage, we use the same UNet as the generator with a feature dimension of 32, a feature multiplicity of $[2, 4]$, an attention resolution of $[16]$. For DP-LDM and DP-LoRA, we use the same UNet as the generator with a feature dimension of 32, a feature multiplicity of $[1, 2, 4]$, and an attention resolution of $[4, 8, 16]$. The autoencoder of VAE has a feature dimension of 128, a feature multiplicity of $[1, 2]$, and an attention resolution of $[8, 16]$.

B.2.3. Pretraining. There are two widely used pretraining paradigms: conditional and unconditional pretraining. We describe them as follows.

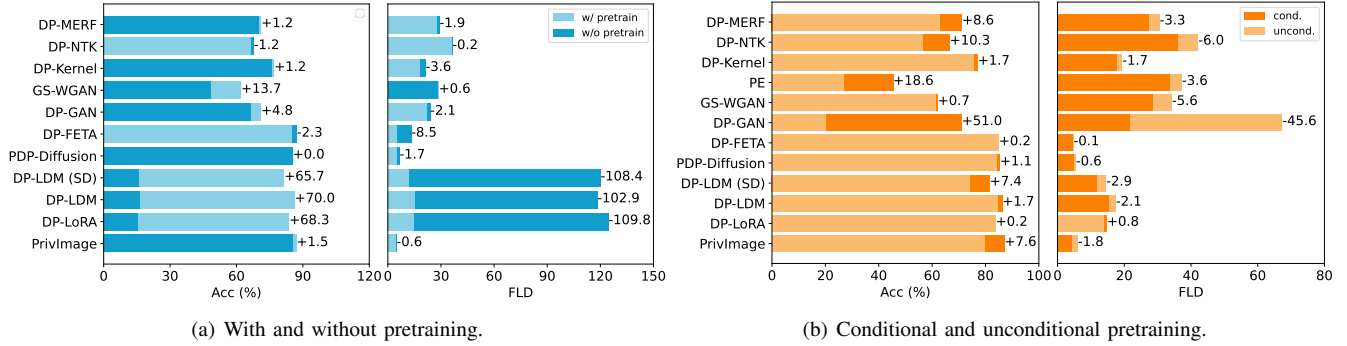


Figure 9: The Acc and FLD evaluations of synthetic images under $\epsilon = 10$ and $\delta = 1/N \log(N)$ for the FashionMNIST dataset. The labels ‘w/ pretrain’ and ‘w/o pretrain’ refer to the studied algorithms with and without pretraining, respectively. ‘cond.’ and ‘uncond.’ indicate the use of conditional and unconditional pretraining. The relative changes indicate the results of w/ pretrain’ minus that of ‘w/o pretrain’, and the result of ‘cond.’ minus that of ‘uncond.’.

- **Conditional:** Given the number of sensitive categories, N_c , the public images must be labeled with one of these categories. For PrivImage, labeling is performed using a semantic query function. For other methods, we randomly assign one of the N_c categories to the public data.
- **Unconditional:** The public data remains unlabeled, and we set the label input as a zero vector.

We base our implementations on the practical code available in the repositories provided by the original papers. In the default setting of DPImageBench, we use conditional pretraining. Table 17 presents the training iterations used for pretraining DP synthesizers across different methods. For methods that do not use a public dataset, we use their default training parameters for pretraining. For methods using a public dataset, we pretrain these methods for 160 epochs with batch size 1,024. Therefore, the pretrain iterations are $1,281,167$ (number of ImageNet images) / $1024 \approx 200,182$. An epoch refers to one complete pass through the entire dataset, while an iteration represents a single training step on a mini-batch. Consequently, for different datasets, it is expected to have a varying number of iterations per epoch due to differences in dataset size. Table 17 presents the hyper-parameters used for pretraining.

B.2.4. Classifier for Utility Evaluation. In utility evaluation, the hyper-parameter settings for the classifiers—ResNet, WideResNet (WRN), and ResNeXt—are adjusted depending on whether the dataset used is CIFAR (including CIFAR-10 and CIFAR-100) or another dataset. For the CIFAR dataset, models are trained with a batch size of 126 for up to 200 epochs, utilizing the SGD optimizer with a learning rate of 0.1, momentum of 0.9, and weight decay of $5e-4$. The learning rate is controlled using a StepLR scheduler with a step size of 60 and a gamma of 0.2. Specifically, WRN is configured with a depth of 28 and a widen factor of 10, ResNet uses a depth of 164 with BasicBlock modules, and ResNeXt uses a depth of 28, a cardinality of 8, and a widen factor of 10, each with a dropout rate of 0.3. For other datasets, the models are trained

with a batch size of 256 for 50 epochs, using the Adam optimizer with a learning rate of 0.01. In these cases, the StepLR scheduler has a step size of 20 and a gamma of 0.2. WRN maintains a dropout rate of 0.3, with a depth of 40 and a widened factor of 4, while ResNet is adjusted to a depth of 110. Across all models, an exponential moving average with a decay rate of 0.9999 is used to enhance training stability.

B.2.5. Metrics for Fidelity Evaluation. We refer to the open-source repository⁵ for implementing FID, IS, Precision, Recall, and FLD metrics. For the human-perspective metric, ImageReward, we refer to the implementation provided at the official repository⁶ of the original paper. Since ImageReward requires the prompt of each image and all the sensitive datasets we investigated do not contain the prompts, we manually design the prompt templates based on the category of the images. For MNIST, the prompt is “A grayscale image of a handwritten digit [label]”. For F-MNIST, the prompt is “A grayscale image of a/an [label]”. For CIFAR-10 and CIFAR-100, the prompt is “An image of a/an [label]”. For EuroSAT, the prompt is “A remote sensing image of a/an [label]”. For CelebA, the prompt is “An image of a [label] face”. For Camelyon, the prompt is “A normal lymph node image” and “A lymph node histopathology image”. Notably, all experiments are conducted using the default hyper-parameters provided in the respective repositories.

B.2.6. Privacy Cost for Hyper-Parameter Tuning. Current DP image synthesis methods overlook the privacy cost associated with hyper-parameter tuning [4], [5], [31], [32]. DPImageBench follows them and similarly does not account for this cost. To mitigate the impact of neglecting privacy loss during hyper-parameter tuning, we should minimize the hyper-parameter tuning process as much as possible. Therefore, we follow the default hyper-parameters the same as that released in the repository as introduced in Section B.

5. <https://github.com/marcojira/FLD>

6. <https://github.com/THUDM/ImageReward>

TABLE 18: Fidelity evaluations for the Camelyon dataset.

Algorithm	Camelyon					
	FID↓	IS↑	Precision↑	Recall↑	FLD↓	IR↑
DP-MERF	251.6	2.45	0.12	0.00	50.5	-2.16
DP-NTK	234.5	1.67	0.00	0.00	52.7	-2.25
DP-Kernel	217.3	3.21	0.01	0.01	38.0	-2.21
PE	69.1	4.58	0.01	0.77	13.6	-2.11
GS-WGAN	291.8	1.45	0.04	0.01	64.2	-2.27
DP-GAN	66.9	1.84	0.37	0.14	3.01	-1.67
DPDM	29.2	1.65	0.74	0.29	-2.71	-1.87
DP-FETA	27.8	1.69	0.72	0.31	-4.4	-1.84
PDP-Diffusion	6.1	2.09	0.62	0.69	-5.9	-1.82
DP-LDM (SD)	15.3	2.03	0.46	0.68	-4.22	-1.92
DP-LDM	45.4	1.88	0.32	0.43	-0.21	-1.91
DP-LoRA	36.8	1.94	0.35	0.51	-5.09	-1.91
PrivImage	10.1	2.17	0.50	0.71	-4.76	-1.88

Besides, different synthesis methods often use the same value for shared hyper-parameters when applied to the same synthesis task. The results could be further improved with optimized hyper-parameters beyond those we used.

Appendix C. Details Descriptions of Datasets

We evaluate DPImageBench on seven sensitive datasets: (1) MNIST [64], (2) FashionMNIST [65], (3) CIFAR-10 [66], (4) CIFAR-100 [66], (5) EuroSAT [67], (6) CelebA [43], and (7) Camelyon [42]. Besides, the ImageNet ISLVR2012 [59], MS COCO, and LAION [77] datasets are considered a public dataset. This section introduces the investigated dataset as follows.

- **MNIST:** The MNIST (Modified National Institute of Standards and Technology) has 70,000 grayscale images of handwritten digits (0-9), with 60,000 images for training and 10,000 for testing. Each image is 28×28 pixels.
- **FashionMNIST:** This dataset contains 70,000 grayscale images of fashion items divided into 10 categories (including t-shirts, trousers, shoes, and bags). Each image is 28×28 pixels in size, similar to the original MNIST dataset, but featuring clothing and accessories.
- **CIFAR-10:** CIFAR-10 contains 60,000 color images, each with a resolution of 32×32 pixels, categorized into 10 different classes: airplanes, cars, birds, cats, deer, dogs, frogs, horses, ships, and trucks.
- **CIFAR-100:** It contains 60,000 color images, each with a resolution of 32×32 pixels. It is organized into 100 classes. These classes are further grouped into 20 superclasses, each comprising several related subclasses (the superclasses “animals” include subclasses like “beaver.”).
- **EuroSAT:** This dataset comprises diverse satellite images optimized for land use and land cover classification tasks. EuroSAT contains 10 distinct classes, including forests, rivers, and urban environments. EuroSAT features over 27,000 labeled and georeferenced images, each measuring 64×64 pixels, capturing a broad spectrum of geographical and environmental scenarios across Europe.
- **CelebA:** The CelebA (CelebFaces Attributes) dataset contains over 200,000 color celebrity images, each with a resolution of 128×128 pixels and annotated with 40

binary attributes, including features such as “smiling,” “young,” “wearing glasses,” “blond hair,” and more.

- **Camelyon:** The Camelyon dataset is a large-scale medical imaging resource aimed at advancing research in digital pathology, particularly for the detection of metastatic cancer in lymph node tissue sections. It consists of high-resolution histopathological images, known as whole-slide images, of lymph node samples. Each image in the Camelyon dataset is meticulously annotated by expert pathologists, marking the regions where cancer is present.
- **ImageNet ISLVR2012:** ImageNet Large Scale Visual Recognition Challenge (ISLVR) 2012 contains over 14 million images labeled across 1,000 object categories, including animals, vehicles, and others. Each image has a resolution of 256×256 pixels. We use a subset of the whole ImageNet dataset for pretraining like previous works [4], [32]. This subset of the dataset is specifically used for the ImageNet Large Scale Visual Recognition Challenge.
- **Places365:** The Places365 dataset is a large-scale scene recognition dataset designed to support visual recognition research. It contains over 1.8 million images categorized into 365 scene classes, such as beaches, kitchens, and libraries, providing a diverse collection of places encountered in everyday environments.

Appendix D. Additional Experiments Analysis

Fidelity Evaluations of Camelyon Dataset. Table 18 shows the fidelity results for various methods on the Camelyon dataset. PE achieves the highest IS score of 4.58 among the studied methods. However, the downstream task accuracy achieved by PE is only 64.9%. These results indicate that although PE can generate images with high practical quality, they are not similar to sensitive images. The precision and recall values of 0.01 and 0.77 further support this perspective. Besides, the FLD of synthetic images achieved by PDP-Diffusion and PrivImage are both negative, i.e., -5.9 and -5.09, suggesting that, according to this metric, the quality of the synthetic images surpasses that of the original images. Additionally, the accuracy achieved by PDP-Diffusion and PrivImage is 84.8% and 87.0%, respectively, which closely approaches the accuracy obtained on the original dataset, i.e., 87.7%.

The Impact of Pretraining. Figure 9 presents the Acc and FLD evaluations of synthetic images under $\epsilon = 10$ for the FashionMNIST dataset.

Computational Resources. All methods are implemented on a server equipped with four NVIDIA GeForce A6000 Ada GPUs and 512GB of memory. The synthesizer sizes for the GAN-based and diffusion-based methods are 5.6M and 3.8M. For GAN, the generator size is 3.8M, and the discriminator size is 1.8M. Consistently shared hyper-parameters are used across all methods, as outlined in Appendix B.2.1.

Table 19 provides an analysis of GPU memory usage and runtime for the methods studied in DPImageBench using the CIFAR-10 dataset. Overall, the diffusion-based synthesizer

TABLE 19: GPU memory usage and runtime analysis of studied methods in DPImageBench for the CIFAR-10.

Algorithm	Stage	Memory	Runtime	Max Memory
DP-MERF	Pretrain	0 GB	0 H	18.6 GB
	Fine-tune	3.5 GB	0.02 H	
	Synthesis	18.6 GB	0.03 H	
DP-NTK	Pretrain	0 GB	0 H	21.3 GB
	Fine-tune	4.8 GB	7.75 H	
	Synthesis	19.1 GB	0.05 H	
DP-Kernel	Pretrain	0 GB	0 H	22.5 GB
	Fine-tune	8.8 GB	3.6 H	
	Synthesis	19.0 GB	0.05 H	
PE	Pretrain	0 GB	0 H	183.0 GB
	Fine-tune	0 GB	0 H	
	Synthesis	183.0 GB	12.0 H	
GS-WGAN	Pretrain	21.6 GB	18.3 H	21.6 GB
	Fine-tune	21.6 GB	0.6 H	
	Synthesis	20.0 GB	0.01 H	
DP-GAN	Pretrain	0 GB	0 H	46.1 GB
	Fine-tune	46.1 GB	3.25 H	
	Synthesis	20.1 GB	0.03 H	
DPDM	Pretrain	0 GB	0 H	96.3 GB
	Fine-tune	96.3 GB	20.5 H	
	Synthesis	32.1 GB	0.17 H	
DP-FETA	Pretrain	3.4 GB	7.2 H	96.3 GB
	Fine-tune	96.3 GB	20.5 H	
	Synthesis	32.1 GB	0.17 H	
PDP-Diffusion	Pretrain	34.3 GB	32.0 H	96.3 GB
	Fine-tune	96.3 GB	20.5 H	
	Synthesis	32.1 GB	0.17 H	
DP-LDM (SD)	Pretrain	34.3 GB	32.0 H	96.3 GB
	Fine-tune	60.0 GB	9.1 H	
	Synthesis	32.1 GB	0.17 H	
DP-LDM	Pretrain	40.0 GB	75.0 H	40.0 GB
	Fine-tune	20.8 GB	2.5 H	
	Synthesis	5.8 GB	0.5 H	
DP-LORA	Pretrain	40.0 GB	75.0 H	40.0 GB
	Fine-tune	35.6 GB	20.5 H	
	Synthesis	5.8 GB	0.5 H	
PrivImage	Pretrain	34.3 GB	32.0 H	96.3 GB
	Fine-tune	96.3 GB	20.5 H	
	Synthesis	32.1 GB	0.17 H	

requires more GPU resources and has a longer runtime compared to the GAN-based methods. In fact, the computation resource cost heavily depends on multiple factors, like the size of the synthesizer parameters, the batch size, etc. We recommend using the largest possible batch size for finetuning the synthesizers, while it needs more computation resources. However, with the same privacy budget, using a larger batch size results in a smaller scale of DP noise being added during finetuning for each individual image [52], which can lead to improved synthesis results.

Appendix E. Error in DP-Promise

DP-Promise [24] proposes reducing the noise introduced by DP during training for highly efficient training. We argue that *the DP-Promise does not strictly satisfy DP*. In DMs, as introduced in Section 2.2, the image is gradually corrupted with noise until it becomes random noise, while a neural network is trained to reverse this process and recover the original image. DP-Promise proposes achieving DP by utilizing the noisy process in DM. Specifically, in the forward

process of DMs, we add noise to the image x_0 through $x_t = \sqrt{\bar{\alpha}_t}x_0 + e\sqrt{1 - \bar{\alpha}_t}$, where $\bar{\alpha}_t$ ⁷ is a fixed hyperparameter, e indicates the added noise, and x_t is the noisy image. They theoretically prove that this process naturally satisfies DP with ϵ as the DP noise, and its privacy cost decreases as t increases. Thus, when t is sufficiently large, we do not need to introduce additional noise to the gradient. However, the analysis of DP-Promise overlooks the fact that, in addition to x_t , the training also has access to the noise e (DP noise should be unknown) and the time step t to calculate the objective function 4. If e and t are not added with noise, we can easily reconstruct the original image x_0 via $x_0 = (x_t - e\sqrt{1 - \bar{\alpha}_t})/\sqrt{\bar{\alpha}_t}$ (by inverting Eq (3)). Therefore, we believe that DP-Promise violates DP, and we do not implement DP-Promise in DPImageBench.

7. $\bar{\alpha}_t$ is required for both training DMs and generating images.